Using PCA in Time-of-Flight Vectors for Reflector Recognition and 3-D Localization

J. A. Jiménez, M. Mazo, *Member, IEEE*, J. Ureña, A. Hernández, F. Álvarez, J. J. García, and E. Santiso

***Abstract*—This paper presents a reflector recognition and localization technique in three-dimensional (3-D) environments, using only times-of-flight (TOFs) data obtained from ultrasonic transducers. The recognition and localization technique is based on the principal component analysis applied to the TOF vectors originating from a sensor that contains two emitting transducers and several receivers. The two emitters simultaneously transmit two coded pulses that are detected later on and discriminated by the receivers, after being reflected in the environment. The proposed technique allows for the possibility of not only recognizing the reflectors, but also estimating approximately its localization referred to the sensor. This technique has been tested with three types of reflectors in 3-D environments: planes, edges, and corners. The achieved results are very satisfactory for reflectors located in the range 50–350 cm.**

***Index Terms*—Principal component analysis (PCA), reflector classification, three-dimensional (3-D) localization, times-of-flight (TOFs), ultrasonic sensors.**

I. Introduction

PAST research about ultrasonic applications for mobile robots has focused on the classification of some basic reflectors. The more interesting basic reflectors in mobile robotics are planes, edges, and corners, since these three types of natural marks are usually found in indoor environments where robots move [1]–[4]. The reflector identification and localization constitutes a fundamental task inside mobile robotics, since this information contributes in a decisive way to other higher level tasks, such as the generation of environment maps and the mobile robot's localization.

Using the received echoes, different characteristics can be obtained: times-of-flight (TOFs), width of the echo signal, length of the echo, frequency components, etc. [5], [6]. The reflector classification can be carried out using one or several of these characteristics. The most common alternatives are those that exclusively analyze the TOFs [4], [7]–[10], those that exclusively measure the amplitude of the received echoes [2], [11]–[13], those that combine both [6], [14]–[17], and those that combine different characteristics such as amplitude, frequency, phases, TOFs, etc. [18], [33]. Among the different alternatives, the one most often used in mobile robotics is the one that uses TOFs exclusively, since these have a more reduced dependence from the environmental variations (temperature, humidity, air flows, etc.), and the execution times are smaller, mainly compared with other alternatives that use a high number of characteristics. In this paper, only TOFs are used to carry out the reflector classification and localization.

Another important aspect related to the reflector recognition is the possibility of obtaining two-dimensional (2-D) or three-dimensional (3-D) information about them. In the first case (2-D classification), reflectors in the environment are projected on the plane where the transducers are. This simplification has the inconvenience that false interpretations can take place, since some reduced information about the reflectors is obtained. The 3-D recognition systems provide realistic information about reflectors in the environment, which implies an improvement in the mobile robot's positioning tasks, and they also make easier the possible fusion with other types of sensors that also provide 3-D information from the environment.

For classification tasks, several ultrasonic transducers are often grouped, forming an ultrasonic sensor. The design and configuration of the sensor also requires a careful study, since the obtained information depends on it. This information is closely related to the spatial configuration of the transducers forming the sensorial structure, to the emission/reception functions assigned to the different transducers (emitters, receivers, and emitter/receivers), to the possibility of carrying out simultaneous emissions by several transducers without crosstalk problems, and to the number of transducers used as receivers. In this way, for example, the capacity to classify different reflector types and the possibility of obtaining 2-D or 3-D information depends on the spatial sensor configuration. In mobile robot applications, it is also very important to carry out simultaneous measurements of different TOFs that allow, after each measurement and without stopping the robot, carrying out the reflector classification.

For the classification in 2-D, sensorial structures, formed by linear arrays of two, three, or four transducers, are usually used. One of the first contributions on the classification of 2-D reflectors was developed by Peremans *et al.* [7], where a linear triaural array was used. Here, the central transducer operated as emitter/receiver, and both lateral ones only as receivers. With this structure and using the TOFs obtained after only one emission, it is possible to discriminate between edge and plane reflector types, and to obtain their position (angle and distance).

Manuscript received July 13, 2004; revised January 10, 2005. This paper was recommended for publication by Associate Editor D. Fox and Editor F. Park upon evaluation of the reviewers' comments. This work was supported by the Ministry of Science and Technology under the PARMEI Project (reference DIP2003-08715-C02-01) and under UAH Project ISUAP (PI2004/033).

J. A. Jiménez, M. Mazo, J. Ureña, A. Hernández, J. J. García, and E. Santiso are with the Electronics Department, University of Alcalá, 28806 Madrid, Spain (e-mail: jimenez@depeca.uah.es; mazo@depeca.uah.es; urena@depeca.uah.es; alvaro@depeca.uah.es; jesus@depeca.uah.es; santiso@depeca.uah.es).

F. Álvarez is with the Department of Electronics and Electromechanical Engineering, University of Extremadura, 06071 Badajoz, Spain (e-mail: fafranco@unex.es).

Digital Object Identifier 10.1109/TRO.2005.851375

With this same sensorial structure, carrying out two measurements from different positions, reflectors can be discriminated between plane, edge, and corner types [19]. If a sensor formed by three transducers is used, one operating as emitter/receiver, other as emitter, and the third as receiver, it is possible to carry out the classification of reflector types plane, edge, and corner from only one localization of the sensor [4], but with sequential emissions. In this way, Ureña [20] proposes a sensorial structure formed by four transducers. With respect to the process of reflector classification, the techniques more broadly used are based on geometric considerations obtained from the TOFs for every reflector type. The classification algorithms proposed by other authors are also diverse. For example, Kleeman [4] proposes a maximum-likelihood estimator (MLE), and Ureña [20] proposes a Bayesian statistical classifier. An important inconvenience of the systems based on geometric considerations is their high dependence on the precision with which the measurements of the TOFs are carried out, and consequently, the classification results are strongly influenced by noise.

In the field of 3-D reflector recognition, using only TOFs, and oriented to applications in mobile robotics, there is not much research activity. In this way, Akbarally and Kleeman [21] propose a sensor formed by two structures such as those described by Kleeman and Kuc [4], one mounted in the horizontal direction, and the other one in vertical. The combination of the TOFs obtained by the two structures allows the classification to be carried out. In Hong and Kleeman [22] a sensorial structure is proposed, with the shape of an equilateral triangle in which the vertices have three transducers that are operating as emitters/receivers. In this case, the proposed classification algorithm is an MLE, similar to the one proposed by Kleeman and Kuc [4]. Even though emissions in these papers are not simultaneous, in later ones [9], [31], [32], Kleeman has developed techniques for simultaneous emission.

In this paper, a novel classification and localization technique for 3-D reflectors is presented, only using TOFs and a classifier based on principal components analysis (PCA). The PCA technique can be used in several application fields, such as face recognition [34], voice processing [35], handwritten-characters recognition [36], and sonar-signal classification [37]. In ultrasonic sensor applications, the recent codification and processing techniques [30] allow simultaneously obtaining multiple TOFs, which justify the use of PCA techniques, since they are strongly correlated.

The proposed classification technique has been called Identification and Localization based on PCA (ILPCA). A new sensorial structure composed of two transducers emitters/receivers and 12 receivers is also proposed; it allows 18 TOFs to be obtained in a simultaneous way. The signals transmitted simultaneously by the two emitters are coded by orthogonal complementary sequence pairs [23], [24], which avoids the crosstalk problems among emissions. The sensor and the proposed technique ILPCA have been used for the classification and localization of three types of reflectors (planes, edges, and corners) in 3-D environments. The obtained results improve upon the previous work, not only in the improved success in the classification, but also in processing time. The obtained results demonstrate the correctness of the sensorial structure and the classification method proposed in mobile robot applications.

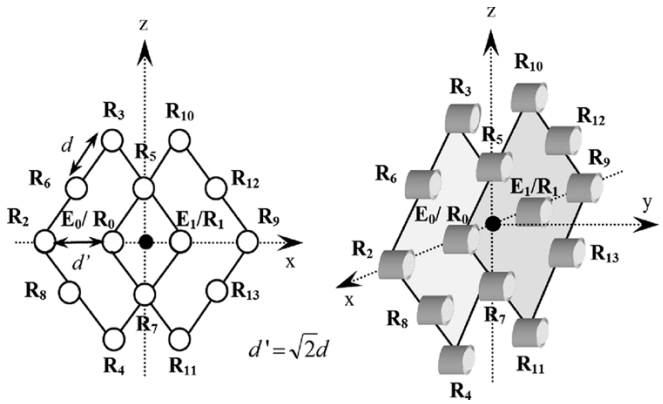

Fig. 1. Proposed sensorial structure.

This paper has been organized in the following sections. In Section II, the proposed sensor is described; in Section III, the proposed ILPCA classification method is explained; Section IV presents the obtained results; and finally, in Section V, the more important conclusions and future work are provided.

II. Sensor

The proposed sensor is formed by 14 transducers, two operating as emitter/receiver and the other twelve only as receivers. In Fig. 1, the geometrical disposition of the different transducers is shown, $\mathrm{E_0/R_0}$ and $\mathrm{E_1/R_1}$ being those working as emitters/receivers, and the remaining ones ($\mathrm{R_2}$ to $\mathrm{R_{13}}$) as receivers. In the proposed sensor, all the transducers are located in the plane $x-z$, with the axial axis in the y direction.

As a remarkable characteristic of the proposed sensor, the possibility of simultaneous emission at emitter $\mathrm{E_0/R_0}$ and $\mathrm{E_1/R_1}$ is found. This is possible because a Golay complementary-sequence pair codes the signal transmitted by each emitting transducer. The Golay sequence pairs $[\mathrm{A_1},\mathrm{B_1}]$ and $[\mathrm{A_2},\mathrm{B_2}]$ used for each emitter are orthogonal between them, $C_{A_1B_1}+C_{A_2B_2}=0$, $C_{A_1B_1}$ and $C_{A_2B_2}$ being the cross-correlations for $\mathrm{A_1}$ and $\mathrm{B_1}$, and $\mathrm{A_2}$ and $\mathrm{B_2}$, respectively. The possibility of using Golay complementary-sequence pairs to determine TOFs has been demonstrated in previous work [23]. In order to allow the discrimination of echoes, depending on the emission source, there exists a low-level electronic system in every receptor for the detection of two different and orthogonal Golay sequence pairs [23] (see Fig. 2). Here, the block diagram for emitter/receiver 1 can be observed: its emission is coded by the pair $[\mathrm{A_1},\mathrm{B_1}]$, and it discriminates echoes from itself or from other emitters (whose emission is coded by the pair $[\mathrm{A_2},\mathrm{B_2}]$). The implementation of the system is described in detail in [24].

The pulses emitted by $\mathrm{E_0/R_0}$ are processed, not only by itself, but also by transducers $\mathrm{E_1/R_1}$ and $\mathrm{R_2}$ through $\mathrm{R_8}$. The pulses emitted by $\mathrm{E_1/R_1}$ are processed by itself $(\mathrm{E_1/R_1})$ and by transducers $\mathrm{E_0/R_0}, \mathrm{R_5}, \mathrm{R_7}, \mathrm{R_9}, \mathrm{R_{10}}, \mathrm{R_{11}}, \mathrm{R_{12}}$, and $\mathrm{R_{13}}$ (see Table I). Therefore, 18 TOFs are computed in every measurement cycle.

The improvement of the proposed sensorial structure, regarding previous work in this field, resides in its capacity

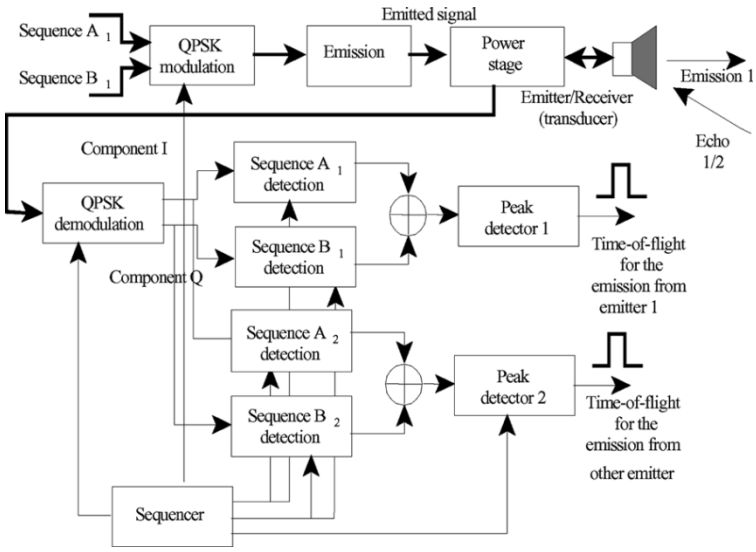

Fig. 2. Simplified scheme of the processing system for an emitter/receiver transducer.

TABLE I
EMISSION/RECEPTION CONFIGURATION FOR TRANSDUCERS IN THE SENSORIAL STRUCTURE

Emitters/Receivers	Receivers
E_0/R_0	E_0/R_0, E_1/R_1, R_2, R_3, R_4, R_5, R_6, R_7, R_8
E_1/R_1	E_0/R_0, E_1/R_1, R_5, R_7, R_9, R_{10}, R_{11}, R_{12}, R_{13}

to obtain 3-D information, and also in the high redundancy provided when obtaining a total of 18 TOFs in a simultaneous way. This implies a higher reliability when carrying out the classification. Also, using the 18 TOFs obtained after every emission, the 3-D reflector classification and localization can be carried out, so this solution is specially suitable for applications in robotics, since all the information to carry out the reflector classification can be obtained from only one robot's position, and with reduced processing times. On the other hand, the geometrical distribution of the transducers presents a great symmetry, which facilitates possible modifications in the number of transducers.

The distance d (see Fig. 1), between transducers, is constrained by their physical dimensions and by the echo correspondence [4], [20]. In this case, $d = 17$ cm has been configured.

III. REFLECTOR RECOGNITION AND LOCALIZATION. ILPCA ALGORITHM

A. Previous Considerations

A classical feature-extraction and data-representation technique, widely used in the areas of pattern recognition and computer vision, is PCA [25]–[29]. PCA techniques, also known as the Karhunen–Loeve expansion, choose a dimensionality-reducing linear projection that maximizes the scatter of all projected samples.

In this paper, the usage of PCA is proposed to carry out the reflector classification using the measurements of TOFs provided by ultrasonic sensors. For that, suppose a sensor that allows several simultaneous emissions to be carried out from several emitting transducers, obtaining n TOFs. This set of n TOFs forms an n-dimensional column TOF vector identified by $\boldsymbol{\tau}$

$$\boldsymbol{\tau} = [t_1 \quad t_2 \quad \dots \quad t_n]^T \tag{1}$$

where $t_1, t_2, \dots, t_n$ are the TOFs associated with every receiver, and the index T means transposed. In the next paragraphs, vectors $\boldsymbol{\tau}$ will be referred to as TOF vectors, and their associated space as TOF space.

Let us consider a training set of s samples of TOF vectors $\{\boldsymbol{\tau}_0, \boldsymbol{\tau}_1, \dots, \boldsymbol{\tau}_{s-1}\}$, taking values in an n-dimensional TOF space. The averaged TOF vectors of the set are defined by

$$\boldsymbol{\Psi} = \frac{1}{s}\sum_{j=0}^{s-1} \boldsymbol{\tau}_j \tag{2}$$

where $\boldsymbol{\Psi} \in \Re^n$. The difference between each TOF vector and the mean value, known as $\boldsymbol{\Phi}_j$ with $(j = 0, 1, 2, \dots, s-1)$, is obtained as

$$\boldsymbol{\Phi}_j = \boldsymbol{\tau}_j - \boldsymbol{\Psi}, \quad j = 0, 1, 2, \dots, s-1. \tag{3}$$

Let us also consider a linear transformation mapping the original n-dimensional TOF space into an m-dimensional feature space, where $m < n$. The new feature vectors $\Omega_j \in \Re^m$ are defined by the following linear transformation:

$$\begin{aligned} \boldsymbol{\Omega}_j &= [\omega_{j1} \quad \omega_{j2} \quad \dots \quad \omega_{jm}]^T \\ &= \mathbf{U}^T \boldsymbol{\Phi}_j \quad j = 0, 1, 2 \dots, s-1 \end{aligned} \tag{4}$$

where $\mathbf{U} \in \Re^{nxm}$ is a matrix with orthonormal columns ($\mathbf{U}$ is the transformation matrix).

If the total scatter matrix $\mathbf{S}_T$ is defined as

$$\mathbf{S}_T = \sum_{j=0}^{s-1} (\boldsymbol{\Phi}_j)(\boldsymbol{\Phi}_j)^T \tag{5}$$

then, after applying the linear transformation $\mathbf{U}^T$, the scatter of the transformed feature vectors $\{\boldsymbol{\Omega}_0, \boldsymbol{\Omega}_1, \dots, \boldsymbol{\Omega}_{s-1}\}$ is

$\mathbf{U}^T\mathbf{S}_T\mathbf{U}$. In PCA, the transformation matrix is chosen to maximize the determinant of the total scatter matrix of the projected samples, i.e.,

$$\mathbf{U}_{\text{opt}} = \arg\max_U |\mathbf{U}^T\mathbf{S}_T\mathbf{U}| = [\mathbf{u}_1 \quad \mathbf{u}_2 \quad \dots \quad \mathbf{u}_m] \tag{6}$$

where $\{\mathbf{u}_k | k = 1, 2, \dots, m\}$ is the set of n-dimensional eigenvectors of $\mathbf{S}_T$ corresponding to the m largest eigenvalues.

Once the transformation matrix $\mathbf{U}_{\text{opt}}$ is determined and given a new TOF vector $\boldsymbol{\tau}$ to be classified, it is transformed into the feature space through (4), using the transformation matrix shown in (6). In this way, the new vector in the feature space will be

$$\boldsymbol{\Omega} = [\omega_1 \quad \omega_2 \quad \dots \quad \omega_m]^T = \mathbf{U}^T\boldsymbol{\Phi} = \mathbf{U}^T(\boldsymbol{\tau} - \boldsymbol{\Psi}) \tag{7}$$

where, simplifying the notation, the index "opt" in $\mathbf{U}$ has been removed, $\boldsymbol{\Psi}$ is the averaged vector for the TOF vectors determined in (2), and $\boldsymbol{\Phi}$ is the TOF vector with null mean value $\boldsymbol{\Phi} = \boldsymbol{\tau} - \boldsymbol{\Psi}$.

The reconstruction of $\boldsymbol{\Phi}$ from the feature space, identified as $\hat{\boldsymbol{\Phi}}$, is carried out by the inverse transformation given by

$$\hat{\boldsymbol{\Phi}} = \hat{\boldsymbol{\tau}} - \boldsymbol{\Psi} = \mathbf{U}\boldsymbol{\Omega} \tag{8}$$

where $\hat{\boldsymbol{\tau}}$ is the TOF estimation after the reconstruction.

The Euclidean distance between $\boldsymbol{\Phi}$ and $\hat{\boldsymbol{\Phi}}$, given in (9), is called the reconstruction error ε

$$\varepsilon_{=} \|\boldsymbol{\Phi} - \hat{\boldsymbol{\Phi}}\|. \tag{9}$$

The Euclidean distance in the feature space between the feature vector for the projected object $\boldsymbol{\Omega}$, and the one for each one of the s training samples projected $\boldsymbol{\Omega}_j$ (with $j = 0, 1, 2, \dots, s-1$), is given by

$$d_j = \|\boldsymbol{\Omega} - \boldsymbol{\Omega}_j\|, \quad j = 0, 1, 2, \dots, s-1. \tag{10}$$

Regarding the classification, for the new feature vector $\boldsymbol{\tau}$, if $\varepsilon \leq \gamma_\varepsilon$, in the case of a small enough reconstruction error threshold γ_ε, $\boldsymbol{\tau}$ will have a great similarity with any of the s training TOF vectors $\{\boldsymbol{\tau}_0, \boldsymbol{\tau}_1, \dots, \boldsymbol{\tau}_{s-1}\}$ used when obtaining the transformation matrix $\mathbf{U}$.

Furthermore, if there exists j so that $d_j \leq \gamma_{\text{d}}$, considering γ_{d} yields a small enough Euclidean distance threshold in the transformed space, this will imply that $\boldsymbol{\tau}$ is close to one of the samples from the training set $\boldsymbol{\tau}_j (j = 0, 1, 2, \dots, s-1)$.

B. Proposed Classification and Localization Algorithm (ILPCA Algorithm)

In this section, a technique is presented based on the use of the PCA for the identification of reflectors (edge, corner, and plane types), as well as their approximated position (distance, angles in azimuth and elevation) with regard to the sensorial structure.

Before carrying out the description of the ILPCA algorithm, some parameters associated with the sensor will be defined, using Fig. 3: a) the emission/reception cone is defined by the azimuth ($\alpha_{\min} \leq \alpha \leq \alpha_{\max}$) and elevation ($\beta_{\min} \leq \beta \leq \beta_{\max}$) angles; b) the measurement range ρ is defined by $\rho_{\min}$ and $\rho_{\max}$; c) inside the perception cone of the sensor, the vector $\vec{r}$, which

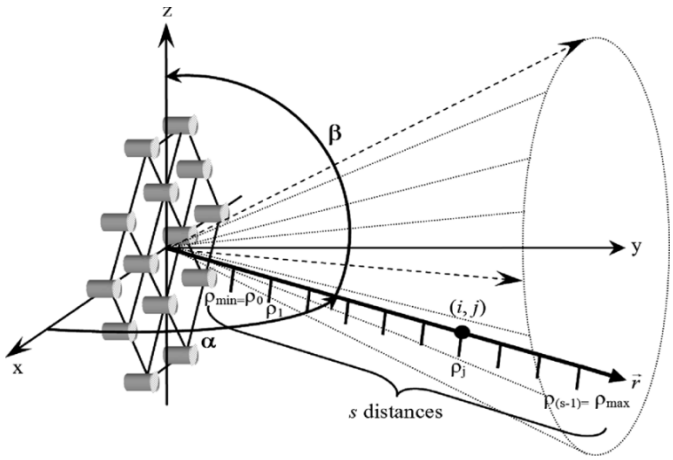

Fig. 3. Perception cone of the proposed sensor.

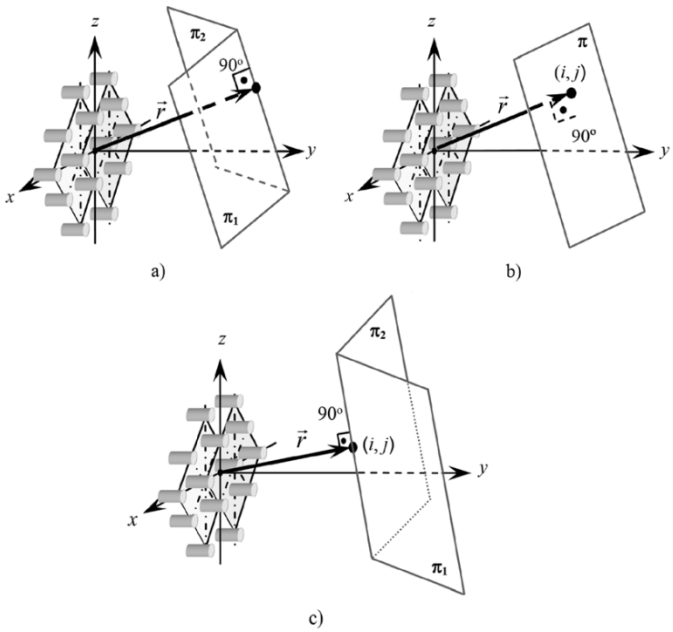

Fig. 4. Position definition for the three reflector types. (a) Corners. (b) Planes. (c) Edges.

defines the position of a reflector, is defined by (ρ, α, β); d) inside the perception cone, q directions are defined (α, β) [these directions are identified by $i (i = 0, 1, \dots, q-1)$]; e) for every direction i, s distances are defined, so they will be referred to as ρ_j, with $j = 0, 1, \dots, s-1$.

In Fig. 4, the three considered reflector types and the definition of the vector $\vec{r}$ are shown. Next, the position vector $\vec{r}$, for q directions and s distances inside the perception cone of the sensor, is determined by (i, j). In the case of corners, the position vector is the one leaving the point (i, j) that is normal to the intersection of the two planes forming it inside their bisector plane, and passing by the coordinate origin of the sensor.

The goal pursued by the ILPCA algorithm is to identify the reflector type, determine the direction i, and to make an approximate estimation of the distance ρ. For that, a class for every reflector type and direction i is defined. The ILPCA algorithm

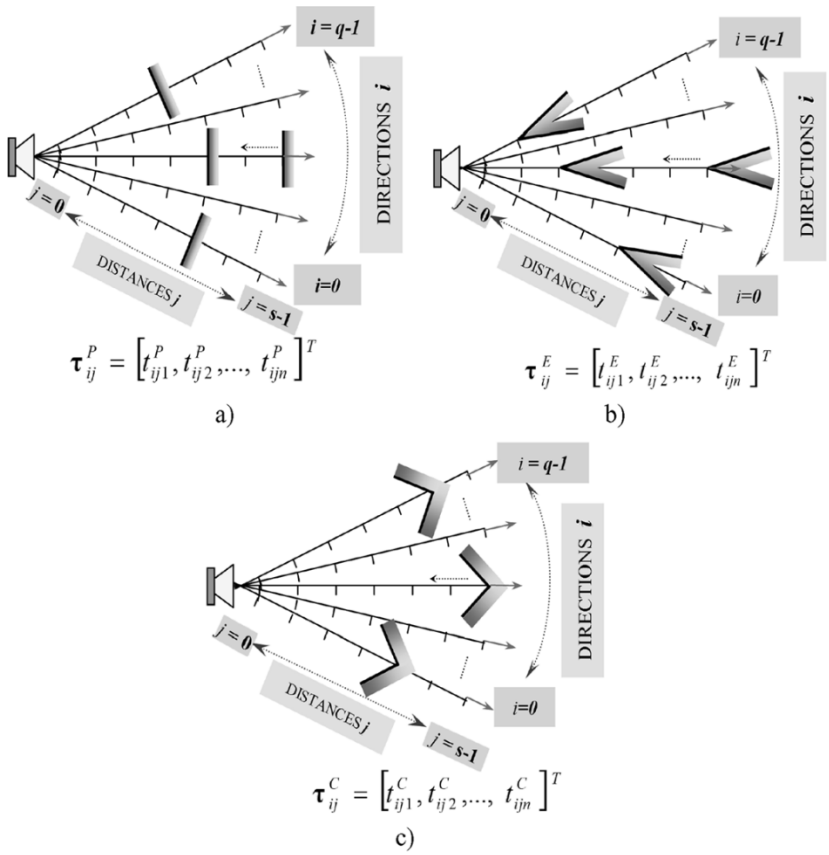

Fig. 5. Example of the localization of training samples for reflectors. (a) Plane type. (b) Edge type. (c) Corner type.

TABLE II
CONSIDERED DIRECTIONS i DEFINED IN FUNCTION OF AZIMUTH AND ELEVATION ANGLES

AZIMUTH \ ELEVATION	-12	-10	-8	-6	-4	-2	0	+2	+4	+6	+8	+10	+12
-12	0	1	2	3	4	5	6	7	8	9	10	11	12
-10	13	14	15	16	17	18	19	20	21	22	23	24	25
-8	26	27	28	29	30	31	32	33	34	35	36	37	38
-6	39	40	41	42	43	44	45	46	47	48	49	50	51
-4	52	53	54	55	56	57	58	59	60	61	62	63	64
-2	65	66	67	68	69	70	71	72	73	74	75	76	77
0	78	79	80	81	82	83	84	85	86	87	88	89	90
+2	91	92	93	94	95	96	97	98	99	100	101	102	103
+4	104	105	106	107	108	109	110	111	112	113	114	115	116
+6	117	118	119	120	121	122	123	124	125	126	127	128	129
+8	130	131	132	133	134	135	136	137	138	139	140	141	142
+10	143	144	145	146	147	148	149	150	151	152	153	154	155
+12	156	157	158	159	160	161	162	163	164	165	166	167	168

associates a transformation matrix with each class. The transformation matrix will be referred to as $\mathbf{U}_{\mathrm{i}}^{P}$, $\mathbf{U}_{\mathrm{i}}^{E}$, and $\mathbf{U}_{\mathrm{i}}^{C}$ for plane, edge, and corner reflectors, respectively, i being the direction of the position vector for the reflector.

The transformation matrices $\mathbf{U}_{\mathrm{i}}^{P}$, $\mathbf{U}_{\mathrm{i}}^{E}$, and $\mathbf{U}_{\mathrm{i}}^{C}$ are generated offline using sets of TOF measurements obtained *a priori*, called training samples. So, for every q considered direction and for every reflector type, s training TOF vectors are obtained in an n-dimensional space of TOFs (in this case, $n = 18$). These n-dimensional TOF vectors obtained in each position (i, j) are referred to as $\boldsymbol{\tau}_{ij}^{P} = [t_{ij1}^{P}, t_{ij2}^{P}, \ldots, t_{ijn}^{P}]$ for planes, $\boldsymbol{\tau}_{ij}^{E} = [t_{ij1}^{E}, t_{ij2}^{E}, \ldots, t_{ijn}^{E}]$ for edges, and $\boldsymbol{\tau}_{ij}^{C} = [t_{ij1}^{C}, t_{ij2}^{C}, \ldots, t_{ijn}^{C}]$ for corners; where the indexes P, E, and C mean the reflector types plane, edge, and corner, respectively. In Fig. 5, a graphical presentation is provided on how the three reflector types have been located to obtain the training TOF vectors. In the case of planes and edges, due to their geometrical characteristics, the pitch angle does not affect the classification. For corners, it has also been tested in simulations that the classification is correct as long as the pitch angle is in the range of $\pm 4^{\circ}$.

The classes $\alpha_{\mathrm{i}}^{P}, \alpha_{\mathrm{i}}^{E}, \alpha_{\mathrm{i}}^{C}$ with $\mathrm{i} = 0, 1, \ldots, q-1$ are obtained for q directions and three reflector types, where $\alpha_{i}^{P}, \alpha_{i}^{E}, \alpha_{i}^{C}$ represent the q classes for every reflector type, plane, edge, and corner, respectively.

Every class $\alpha_{i}^{P}, \alpha_{i}^{E}, \alpha_{i}^{C}$ is characterized by s training TOF vectors

$$\begin{aligned}
\alpha_{i}^{P} &= \left\{\boldsymbol{\tau}_{i0}^{P}, \boldsymbol{\tau}_{i1}^{P}, \ldots, \boldsymbol{\tau}_{i(s-1)}^{P}\right\}, \quad i = 0, 1, \ldots, q-1 \\
\alpha_{i}^{E} &= \left\{\boldsymbol{\tau}_{i0}^{E}, \boldsymbol{\tau}_{i1}^{E}, \ldots, \boldsymbol{\tau}_{i(s-1)}^{E}\right\}, \quad i = 0, 1, \ldots, q-1 \\
\alpha_{i}^{C} &= \left\{\boldsymbol{\tau}_{i0}^{C}, \boldsymbol{\tau}_{i1}^{C}, \ldots, \boldsymbol{\tau}_{i(s-1)}^{C}\right\}, \quad i = 0, 1, \ldots, q-1. \qquad (14)
\end{aligned}$$

If, for every class, the optimum transformation matrix $\mathbf{U}$ is obtained according to (6), and identifying them as $\mathbf{U}_{i}^{P}, \mathbf{U}_{i}^{E}, \mathbf{U}_{i}^{C}, i = 0, 1, \ldots, q-1$, it is concluded that

$$\begin{aligned}
\mathbf{U}_{i}^{P} &= [\mathbf{u}_{i1}^{P} \quad \mathbf{u}_{i2}^{P} \quad \ldots \quad \mathbf{u}_{im}^{P}], \quad i = 0, 1, \ldots, q-1 \\
\mathbf{U}_{i}^{E} &= [\mathbf{u}_{i1}^{E} \quad \mathbf{u}_{i2}^{E} \quad \ldots \quad \mathbf{u}_{im}^{E}], \quad i = 0, 1, \ldots, q-1 \\
\mathbf{U}_{i}^{C} &= [\mathbf{u}_{i1}^{C} \quad \mathbf{u}_{i2}^{C} \quad \ldots \quad \mathbf{u}_{im}^{C}], \quad i = 0, 1, \ldots, q-1 \qquad (15)
\end{aligned}$$

TABLE III
RECONSTRUCTION ERRORS OBTAINED AFTER PROJECTING INTO SPACES CORRESPONDING TO PLANE-TYPE REFLECTORS $\varepsilon_i^P (i = 1, 2, \ldots, 128)$. (a) NEGATIVE ELEVATION ANGLES. (b) POSITIVE ELEVATION ANGLES

AZIMUTH \ ELEVATION	-12	-10	-8	-6	-4	-2	0
-12	0.0008363	0.0008279	0.00082244	0.00082008	0.0008209	0.00082492	0.00083212
-10	0.00073084	0.00071937	0.00071156	0.00070765	0.00070778	0.000712	0.00072025
-8	0.00062515	0.00060982	0.00059902	0.00059314	0.00059245	0.00059703	0.00060678
-6	0.00052077	0.00050037	0.00048555	0.00047702	0.00047528	0.00048051	0.00049251
-4	0.00042042	0.00039303	0.00037237	0.0003599	0.0003567	0.00036315	0.00037882
-2	0.0003296	0.00029217	0.00026218	0.00024287	0.00023719	0.00024631	0.0002688
0	0.00026003	0.00020939	0.00016376	0.00012942	0.0001175	0.00013452	0.00017223
+2	0.00023253	0.00017408	0.00011525	5.6753e-05	**1.6787e-05**	6.7622e-005	0.00012705
+4	0.0002607	0.00021143	0.00016762	0.00013549	0.00012507	0.00014162	0.00017788
+6	0.00032993	0.00029424	0.00026606	0.00024835	0.00024372	0.00025308	0.00027509
+8	0.00041939	0.00039378	0.00037479	0.0003637	0.00036144	0.0003683	0.00038383
+10	0.00051759	0.00049894	0.00048568	0.00047842	0.00047757	0.00048325	0.00049526
+12	0.00061917	0.00060554	0.00059622	0.00059153	0.00059169	0.00059673	0.00060657

a)

AZIMUTH \ ELEVATION	+2	+4	+6	+8	+10	+12
-12	0.00084239	0.00085559	0.00087155	0.00089002	0.00091078	0.00093356
-10	0.0007324	0.00074821	0.00076738	0.00078957	0.00081442	0.00084157
-8	0.00062146	0.00064068	0.00066394	0.00069072	0.00072049	0.00075274
-6	0.00051079	0.00053465	0.00056327	0.0005958	0.00063148	0.00066961
-4	0.0004026	0.00043309	0.00046883	0.00050854	0.00055114	0.0005958
-2	0.00030167	0.00034182	0.00038682	0.00043495	0.00048502	0.00053624
0	0.00022021	0.00027297	0.00032799	0.00038405	0.00044049	0.00049687
+2	0.000187	0.00024695	0.00030667	0.00036601	0.00042484	0.00048305
+4	0.00022447	0.00027607	0.00033014	0.00038539	0.00044112	0.00049687
+6	0.00030701	0.00034601	0.0003898	0.00043673	0.00048566	0.0005358
+8	0.00040702	0.00043658	0.00047117	0.00050961	0.0005509	0.00059422
+10	0.00051314	0.00053624	0.00056383	0.00059514	0.00062946	0.00066616
+12	0.00062095	0.00063953	0.00066187	0.0006875	0.00071594	0.00074674

b)

where $\{\mathbf{u}_{ik}^P | k = 1, 2, \ldots, m\}$, $\{\mathbf{u}_{ik}^E | k = 1, 2, \ldots, m\}$, and $\{\mathbf{u}_{ik}^C | k = 1, 2, \ldots, m\}$ are three n-dimensional eigenvector sets of the scatter matrices $\mathbf{S}_{Ti}^P, \mathbf{S}_{Ti}^E, \mathbf{S}_{Ti}^C$ for every i, respectively. Since these eigenvectors have the same dimension as the original TOF vectors, $\{\mathbf{u}_{ik}^P | k = 1, 2, \ldots, m\}$ are referred to as eigenplanes, $\{\mathbf{u}_{ik}^E | k = 1, 2, \ldots, m\}$ as eigenedges, and $\{\mathbf{u}_{ik}^C | k = 1, 2, \ldots, m\}$ as eigencorners. The scatter matrices $\mathbf{S}_{Ti}^P, \mathbf{S}_{Ti}^E, \mathbf{S}_{Ti}^C$ are given by

$$\mathbf{S}_{Ti}^P = \sum_{j=0}^{s-1} \left(\mathbf{\Phi}_{ij}^P\right)\left(\mathbf{\Phi}_{ij}^P\right)^T$$
$$\mathbf{S}_{Ti}^E = \sum_{j=0}^{s-1} \left(\mathbf{\Phi}_{ij}^E\right)\left(\mathbf{\Phi}_{ij}^E\right)^T$$
$$\mathbf{S}_{Ti}^C = \sum_{j=0}^{s-1} \left(\mathbf{\Phi}_{ij}^C\right)\left(\mathbf{\Phi}_{ij}^C\right)^T \tag{16}$$

where

$$\mathbf{\Phi}_{ij}^P = \boldsymbol{\tau}_{ij}^P - \mathbf{\Psi}_i^P, \quad \mathbf{\Phi}_{ij}^E = \boldsymbol{\tau}_{ij}^E - \mathbf{\Psi}_i^E, \quad \mathbf{\Phi}_{ij}^C = \tau_{ij}^C - \mathbf{\Psi}_i^C \tag{17}$$

$$\mathbf{\Psi}_i^P = \frac{1}{s}\sum_{j=0}^{s-1} \boldsymbol{\tau}_{ij}^P, \quad \mathbf{\Psi}_i^E = \frac{1}{s}\sum_{j=0}^{s-1} \boldsymbol{\tau}_{ij}^E, \quad \mathbf{\Psi}_i^C = \frac{1}{s}\sum_{j=0}^{s-1} \boldsymbol{\tau}_{ij}^C. \tag{18}$$

Once the transformation matrices $\mathbf{U}_i^P$, $\mathbf{U}_i^E$, and $\mathbf{U}_i^C$ with $i = 0, 1, \ldots, q-1$ are obtained and a new n-dimensional TOF vector τ to be classified is given, first the corresponding linear transformations given by (7) are carried out, obtaining $3q$ new feature vectors in the transformed spaces. The feature vectors in the transformed spaces, known as $\mathbf{\Omega}_{\boldsymbol{\tau}i}^P, \mathbf{\Omega}_{\boldsymbol{\tau}i}^E, \mathbf{\Omega}_{\boldsymbol{\tau}i}^C \in \Re^m$, are determined by

$$\begin{aligned}
\mathbf{\Omega}_{\boldsymbol{\tau}i}^P &= \left(\mathbf{U}_i^P\right)^T \mathbf{\Phi}_{\boldsymbol{\tau}i}^P, \quad i = 0, 1, 2 \ldots, q-1 \\
\mathbf{\Omega}_{\boldsymbol{\tau}i}^E &= \left(\mathbf{U}_{\mathrm{i}}^E\right)^T \mathbf{\Phi}_{\boldsymbol{\tau}i}^E, \quad i = 0, 1, 2 \ldots, q-1 \\
\mathbf{\Omega}_{\boldsymbol{\tau}i}^C &= \left(\mathbf{U}_i^C\right)^T \mathbf{\Phi}_{\boldsymbol{\tau}i}^C, \quad i = 0, 1, 2 \ldots, q-1
\end{aligned} \tag{19}$$

being

$$\begin{aligned}
\mathbf{\Phi}_{\boldsymbol{\tau}i}^P &= \boldsymbol{\tau} - \mathbf{\Psi}_i^P, \quad i = 0, 1, \ldots, q-1 \\
\mathbf{\Phi}_{\boldsymbol{\tau}i}^E &= \boldsymbol{\tau} - \mathbf{\Psi}_i^E, \quad i = 0, 1, \ldots, q-1 \\
\mathbf{\Phi}_{\boldsymbol{\tau}i}^C &= \boldsymbol{\tau} - \mathbf{\Psi}_i^C, \quad i = 0, 1, \ldots, q-1
\end{aligned} \tag{20}$$

where $\mathbf{\Omega}_{\boldsymbol{\tau}i}^P, \mathbf{\Omega}_{\boldsymbol{\tau}i}^E, \mathbf{\Omega}_{\boldsymbol{\tau}i}^C \in \Re^m$.

After that, the vectors $\mathbf{\Phi}_{\boldsymbol{\tau}i}^P, \mathbf{\Phi}_{\boldsymbol{\tau}i}^E, \mathbf{\Phi}_{\boldsymbol{\tau}i}^C$ are recovered from every transformed space through the inverse transformation given by (8), obtaining the recovered vectors, known as $\hat{\mathbf{\Phi}}_{\boldsymbol{\tau}i}^P, \hat{\mathbf{\Phi}}_{\boldsymbol{\tau}i}^E, \hat{\mathbf{\Phi}}_{\boldsymbol{\tau}i}^C$

$$\begin{aligned}
\hat{\mathbf{\Phi}}_{\boldsymbol{\tau}i}^P &= \hat{\boldsymbol{\tau}} - \mathbf{\Psi}_i^P = \mathbf{U}_i^P \mathbf{\Omega}_{\boldsymbol{\tau}i}^P, \quad i = 0, 1, \ldots, q-1 \\
\hat{\mathbf{\Phi}}_{\boldsymbol{\tau}i}^E &= \hat{\boldsymbol{\tau}} - \mathbf{\Psi}_i^E = \mathbf{U}_i^E \Omega_{\boldsymbol{\tau}i}^E, \quad i = 0, 1, \ldots, q-1 \\
\hat{\mathbf{\Phi}}_{\boldsymbol{\tau}i}^C &= \hat{\boldsymbol{\tau}} - \mathbf{\Psi}_i^C = \mathbf{U}_i^C \Omega_{\boldsymbol{\tau}i}^C, \quad i = 0, 1, \ldots, q-1.
\end{aligned} \tag{21}$$

TABLE IV
RECONSTRUCTION ERRORS OBTAINED AFTER PROJECTING INTO SPACES CORRESPONDING TO EDGE-TYPE REFLECTORS $\varepsilon_i^E (i = 1, 2, \ldots, 128)$. (a) NEGATIVE ELEVATION ANGLES. (b) POSITIVE ELEVATION ANGLES

AZIMUTH \ ELEVATION	-12	-10	-8	-6	-4	-2	0
-12	0.00084924	0.00084065	0.00083501	0.00083249	0.00083316	0.00083707	0.00084418
-10	0.00074522	0.00073344	0.00072534	0.00072117	0.0007211	0.00072518	0.00073336
-8	0.0006399	0.00062404	0.00061274	0.00060644	0.00060542	0.0006098	0.0006195
-6	0.00053507	0.00051381	0.00049817	0.00048895	0.00048669	0.00049162	0.00050358
-4	0.00043388	0.00040519	0.00038326	0.00036967	0.00036563	0.00037163	0.00038728
-2	0.00034244	0.00030325	0.00027141	0.0002503	0.00024321	0.00025159	0.00027416
0	0.00027326	0.0002208	0.00017305	0.00013618	0.00012156	0.00013708	0.00017506
+2	0.00024727	0.00018772	0.00012826	7.1176e-05	6.6186e-05	7.2989e-005	0.00013108
+4	0.0002768	0.00022664	0.00018197	0.00014881	0.00013665	0.00015113	0.00018629
+6	0.00034689	0.00031036	0.00028124	0.00026253	0.00025689	0.00026541	0.00028692
+8	0.0004369	0.00041065	0.00039099	0.00037924	0.00037639	0.00038277	0.00039802
+10	0.00053506	0.00051601	0.00050232	0.00049465	0.00049344	0.00049882	0.00051064
+12	0.00063575	0.00062187	0.00061228	0.00060734	0.00060726	0.00061211	0.00062179

a)

AZIMUTH \ ELEVATION	+2	+4	+6	+8	+10	+12
-12	0.00085439	0.00086756	0.00088349	0.00090195	0.00092269	0.00094544
-10	0.0007455	0.00076136	0.00078061	0.00080292	0.00082788	0.00085512
-8	0.00063425	0.00065365	0.00067718	0.00070428	0.00073438	0.00076693
-6	0.00052206	0.00054631	0.00057546	0.00060861	0.00064492	0.00068365
-4	0.00041146	0.00044265	0.00047929	0.00052	0.00056362	0.00060922
-2	0.00030776	0.00034908	0.00039546	0.00044503	0.0004965	0.000549
0	0.00022432	0.00027876	0.00033558	0.0003934	0.00045148	0.00050933
+2	0.00019197	0.00025344	0.00031483	0.00037584	0.00043624	0.00049586
+4	0.0002329	0.00028522	0.00034036	0.00039681	0.00045374	0.00051061
+6	0.00031877	0.00035807	0.00040242	0.00045007	0.00049977	0.00055064
+8	0.00042113	0.0004508	0.00048566	0.00052447	0.00056616	0.00060989
+10	0.00052843	0.00055154	0.0005792	0.00061065	0.00064513	0.00068197
+12	0.00063607	0.00065458	0.0006769	0.00070252	0.00073097	0.00076176

b)

Finally, the reconstruction errors defined in (9) are computed

$$\begin{aligned}
\varepsilon_i^P &= \|\boldsymbol{\Phi}_{\boldsymbol{\tau}i}^P - \hat{\boldsymbol{\Phi}}_{\boldsymbol{\tau}i}^P\|, \quad i = 0, 1, \ldots, q-1 \\
\varepsilon_i^E &= \|\boldsymbol{\Phi}_{\boldsymbol{\tau}i}^E - \hat{\boldsymbol{\Phi}}_{\boldsymbol{\tau}i}^E\|, \quad i = 0, 1, \ldots, q-1 \\
\varepsilon_i^C &= \|\boldsymbol{\Phi}_{\boldsymbol{\tau}i}^C - \hat{\boldsymbol{\Phi}}_{\boldsymbol{\tau}i}^C\|, \quad i = 0, 1, \ldots, q-1. \qquad (22)
\end{aligned}$$

The new TOF vector $\boldsymbol{\tau}$ will be classified as belonging to the class associated with the transformation matrix with the smallest reconstruction error, whenever this error is inferior to a certain threshold γ_ε, as is shown in

$$\begin{aligned}
&\textbf{Plane if :} \begin{cases} \varepsilon_{\mathrm{imin}}^P < \varepsilon_{\mathrm{imin}}^E \text{ and } \varepsilon_{\mathrm{imin}}^P < \varepsilon_{\mathrm{imin}}^C & \forall \mathrm{i} \\ \varepsilon_{\mathrm{imin}}^P \le \gamma_\varepsilon \end{cases} \\
&\textbf{Edge if :} \begin{cases} \varepsilon_{\mathrm{imin}}^E < \varepsilon_{\mathrm{imin}}^P \text{ and } \varepsilon_{\mathrm{imin}}^E < \varepsilon_{\mathrm{imin}}^C & \forall \mathrm{i} \\ \varepsilon_{\mathrm{imin}}^E \le \gamma_\varepsilon \end{cases} \\
&\textbf{Corner if :} \begin{cases} \varepsilon_{\mathrm{imin}}^C < \varepsilon_{\mathrm{imin}}^P \text{ and } \varepsilon_{\mathrm{imin}}^C < \varepsilon_{\mathrm{imin}}^E & \forall \mathrm{i} \\ \varepsilon_{\mathrm{imin}}^C \le \gamma_\varepsilon \end{cases} \\
&\text{Other cases} \longrightarrow \text{Indeterminate.} \qquad (23)
\end{aligned}$$

The value of the index i with the minimum reconstruction error indicates the most approximated direction in which the reflector to be classified will be. This value i is referred to as i_a.

Once known, the reflector type (plane, edge, or corner) and the direction i_a at which it is pointed, as well as its distance $\rho_{i_a j} (0 \le j \le s-1)$ referred to the sensorial structure, can be determined in an approximate way. For that, the Euclidean distances in the transformed space between the feature vector for the object τ to be classified, and every feature vector of the training samples of the class to which this reflector belongs, are calculated. For example, if the object $\boldsymbol{\tau}$ was classified as a plane in the direction i_a, the TOF vector set used offline to generate the transformation matrix will have been $\{\boldsymbol{\tau}_{i_\mathrm{a}0}^P, \boldsymbol{\tau}_{i_\mathrm{a}1}^P, \ldots, \boldsymbol{\tau}_{i_\mathrm{a}(s-1)}^P\}$. Therefore, it is only necessary to compute the Euclidean distance in the transformed space among the feature vector corresponding to the TOF vector $\boldsymbol{\tau}$, and the feature vectors corresponding to the training samples, as is shown in

$$d_{i_a j} = \left\| \boldsymbol{\Omega}_{\boldsymbol{\tau}i_\mathrm{a}}^P - \boldsymbol{\Omega}_{i_\mathrm{a}j}^P \right\|, \quad j = 0, 1, \ldots, s-1 \qquad (24)$$

being

$$\begin{aligned}
\boldsymbol{\Omega}_{\boldsymbol{\tau}i_\mathrm{a}}^P &= \left(\mathbf{U}_{i_\mathrm{a}}^P\right)^T \left(\boldsymbol{\tau} - \boldsymbol{\Psi}_{i_\mathrm{a}}^P\right) \\
\boldsymbol{\Omega}_{i_\mathrm{a}j}^P &= \left(\mathbf{U}_{i_\mathrm{a}}^P\right)^T \left(\boldsymbol{\tau}_{i_\mathrm{a}j}^P - \boldsymbol{\Psi}_{i_\mathrm{a}}^P\right), \quad j = 0, 1, \ldots, s-1. \qquad (25)
\end{aligned}$$

TABLE V
RECONSTRUCTION ERRORS OBTAINED AFTER PROJECTING INTO SPACES CORRESPONDING TO CORNER-TYPE REFLECTOR $\varepsilon_i^C (i = 1, 2, \ldots, 128)$. (a) NEGATIVE ELEVATION ANGLES. (b) POSITIVE ELEVATION ANGLES

AZIMUTH \ ELEVATION	-12	-10	-8	-6	-4	-2	0
-12	0.00085642	0.00084707	0.00084087	0.00083795	0.0008384	0.00084226	0.00084948
-10	0.00074866	0.00073626	0.0007277	0.00072323	0.00072299	0.00072702	0.00073529
-8	0.00064059	0.0006243	0.00061274	0.00060628	0.00060519	0.00060956	0.0006193
-6	0.00053386	0.00051245	0.00049681	0.00048765	0.00048547	0.00049045	0.00050241
-4	0.00043141	0.0004029	0.00038132	0.00036811	0.00036438	0.00037051	0.0003861
-2	0.00033907	0.0003004	0.00026934	0.00024911	0.00024269	0.00025134	0.0002737
0	0.00026912	0.00021733	0.00017073	0.0001355	0.00012247	0.0001384	0.0001757
+2	0.0002427	0.00018363	0.00012509	6.9772e-005	5.8902e-005	7.5319e-005	0.00013187
+4	0.00027267	0.00022284	0.00017885	0.0001467	0.0001356	0.00015057	0.00018551
+6	0.0003439	0.00030744	0.00027863	0.00026034	0.00025509	0.00026381	0.00028529
+8	0.00043554	0.00040907	0.00038935	0.00037766	0.00037488	0.00038133	0.00039659
+10	0.000536	0.00051646	0.00050245	0.0004946	0.00049329	0.00049866	0.00051052
+12	0.00063982	0.00062526	0.00061518	0.0006099	0.00060963	0.00061442	0.00062417

a)

AZIMUTH \ ELEVATION	+2	+4	+6	+8	+10	+12
-12	0.00085998	0.00087361	0.0008902	0.00090951	0.00093131	0.00095535
-10	0.00074763	0.00076383	0.0007836	0.00080659	0.00083246	0.00086083
-8	0.00063416	0.00065374	0.00067758	0.00070515	0.00073593	0.0007694
-6	0.00052085	0.00054508	0.00057429	0.00060764	0.00064436	0.00068375
-4	0.00041005	0.00044095	0.00047735	0.00051796	0.00056169	0.00060769
-2	0.00030678	0.00034746	0.00039325	0.00044242	0.00049375	0.00054644
0	0.00022392	0.00027732	0.00033328	0.0003905	0.00044829	0.00050623
+2	0.00019145	0.00025183	0.00031237	0.00037281	0.00043296	0.00049269
+4	0.00023154	0.00028321	0.00033779	0.0003939	0.00045076	0.0005079
+6	0.00031694	0.00035598	0.00040015	0.00044776	0.00049765	0.00054901
+8	0.0004197	0.00044939	0.00048436	0.00052343	0.0005656	0.00061006
+10	0.00052843	0.00055176	0.00057978	0.00061174	0.00064695	0.00068475
+12	0.00063866	0.00065754	0.00068038	0.00070673	0.0007361	0.00076803

b)

TABLE VI
EUCLIDEAN DISTANCE IN TRANSFORMED SPACE BETWEEN FEATURE VECTORS FOR THE PATTERN REFLECTORS OF THE PLANE CLASS WITH AZIMUTH $+2^\circ$ AND ELEVATION -4°, AND FEATURE VECTOR FOR THE REFLECTOR TO BE CLASSIFIED, CONSIDERING MEASUREMENTS WITH TYPICAL NOISE DEVIATION OF 5 μs

$\rho_{i_a j}$ (cm)	50	80	110	140	170	200	230	260	290	320	350
$d_{i_a j}$	0.0272	0.0198	0.0124	0.0049	0.0024	0.0099	0.0174	0.024	0.0324	0.0399	0.0473

$\rho_{i_a j}$ = Distances at which reflectors have been placed in cm.

$d_{i_a j}$ = Euclidean distances in the transformed space between the feature vectors of the pattern reflectors and the vector of the object to be classified. $d_{i_a j} = \left\| \mathbf{\Omega}_{\tau j}^P - \mathbf{\Omega}_{i_a j}^P \right\|$ with (j = 0, 1, 2, .., 11).

The value $\rho_{i_a j}$ corresponding to the value j, that provides the minimum $d_{i_a j}$, will be the approximate reflector distance, in the direction i_a.

It has been proven empirically that the relationship among the distances of the reflectors to the sensorial structure, and the Euclidean distances of their feature vectors in the transformed space, is approximately linear. In this way, considering the distance interval, where the reflector is, and the Euclidean distances in the transformed space, a correct estimation can be obtained by means of a linear interpolation in the distance at which the reflector is positioned. For instance, if the feature vector for the reflector to be classified in the transformed space, referred to as

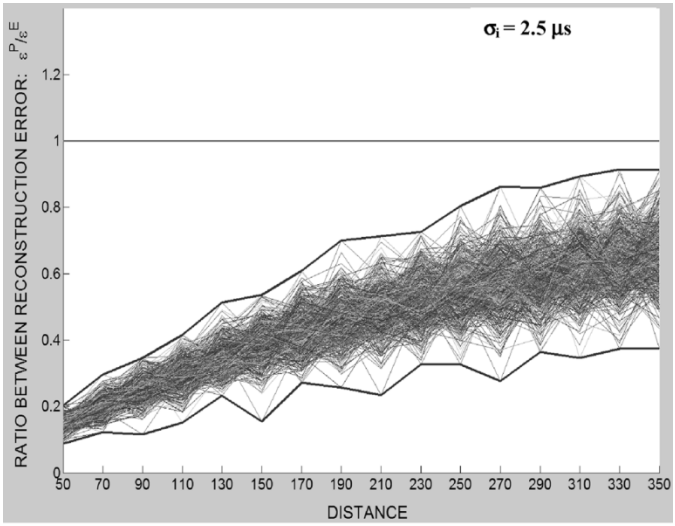

a)

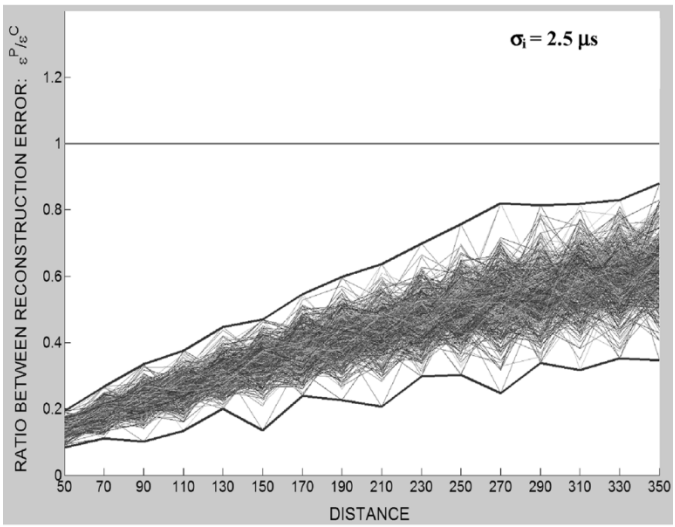

b)

Fig. 6. Ratios between reconstruction errors (a) $\varepsilon^P_{i_{\min}}/\varepsilon^E_{i_{\min}}$ and (b) $\varepsilon^P_{i_{\min}}/\varepsilon^C_{i_{\min}}$ for plane-type reflector.

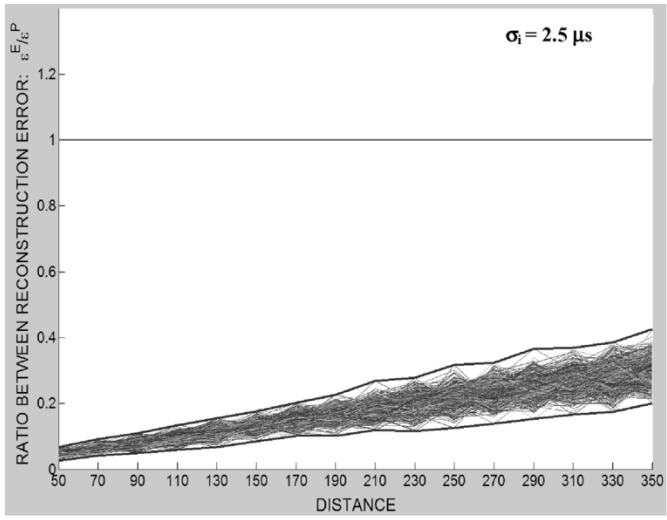

a)

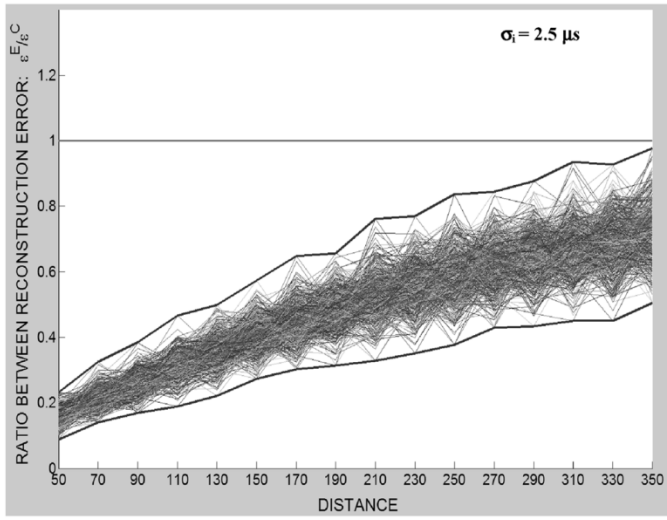

b)

Fig. 7. Ratios between reconstruction errors (a) $\varepsilon^E_{i_{\min}}/\varepsilon^P_{i_{\min}}$ and (b) $\varepsilon^E_{i_{\min}}/\varepsilon^C_{i_{\min}}$ for edge-type reflector.

$\mathbf{\Omega}_{\boldsymbol{\tau} i_a}$, is inside the interval between $\mathbf{\Omega}_{i_a j_a}$ and $\mathbf{\Omega}_{i_a(j_a+1)}$, the approximated distance at which the reflector is, is defined by

$$\rho = \rho_{\mathbf{i_a}j_a} + \frac{\rho_{\mathbf{i_a}(j_a+1)} - \rho_{\mathbf{i_a}(j_a)}}{\left\|\mathbf{\Omega}_{\mathbf{i_a}(j_a+1)} - \mathbf{\Omega}_{\mathbf{i_a}j_a}\right\|} \left\|\mathbf{\Omega}_{\boldsymbol{\tau}\mathbf{i_a}} - \mathbf{\Omega}_{\mathbf{i_a}j_a}\right\| \quad (27)$$

$\rho_{i_a j_a}$ being the distance to the nearest pattern reflector, and $\rho_{i_a(j_a-1)}$ and $\rho_{i_a(j_a+1)}$ the previous and following distances to $\rho_{i_a j_a}$, respectively.

IV. Results

With the purpose of checking the efficacy of the algorithm described in the previous section, diverse experimental tests have been realized. As a previous step to these, while trying to verify the behavior of the algorithm, several simulations have been carried out. In order to carry out the simulations, a simulator has been used; this allows TOFs to be obtained in 3-D environments, based on the rays technique. Concerning the number of principal components to be used, with two principal components (the most significant eigenvalues), good results are obtained; nevertheless, these are significantly improved when three principal components are considered. Using more than three components does not improve the results too much. Anyway, a large number of components implies a higher computation load, thus three components were used as a commitment between accuracy and computation time. In these conditions, the computation time, using a TI 6701 DSP, to carry out a whole classification over a set of 507 classes (169 spatial directions for each three reflector kinds) is 11 ms.

A. Simulated Results

The training samples for every reflector type have been obtained, as was noted previously, which were located at different distances and directions. Every considered direction i is defined by the values of the azimuth and elevation angles. In particular, the reflectors have been located at distances from 50 to 350 cm, with 30-cm intervals. Therefore, the transformation matrices $\mathbf{U}_i^P$, $\mathbf{U}_i^E$, and $\mathbf{U}_i^C$, in every direction i, are obtained from $s = 11$ patterns. With regard to the directions, azimuth angles from -12^o to $+12^o$, with 2^o intervals, have been considered,

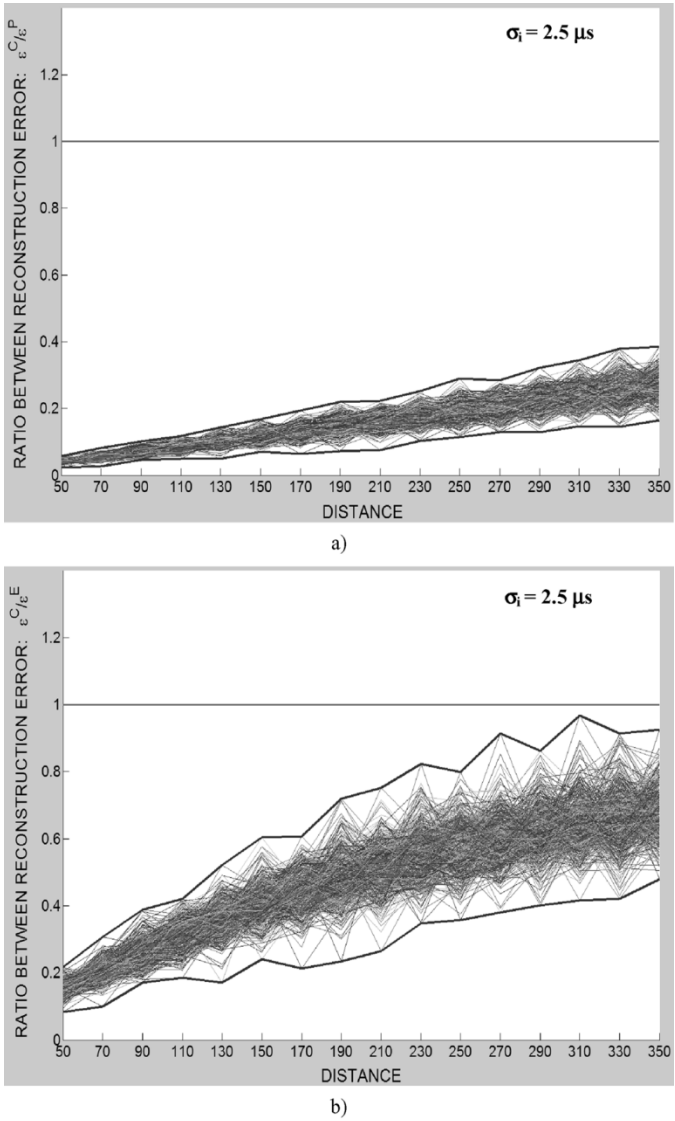

Fig. 8. Ratios between reconstruction errors (a) $\varepsilon^C_{i_{\min}}/\varepsilon^P_{i_{\min}}$ and (b) $\varepsilon^C_{i_{\min}}/\varepsilon^E_{i_{\min}}$ for corner-type reflector.

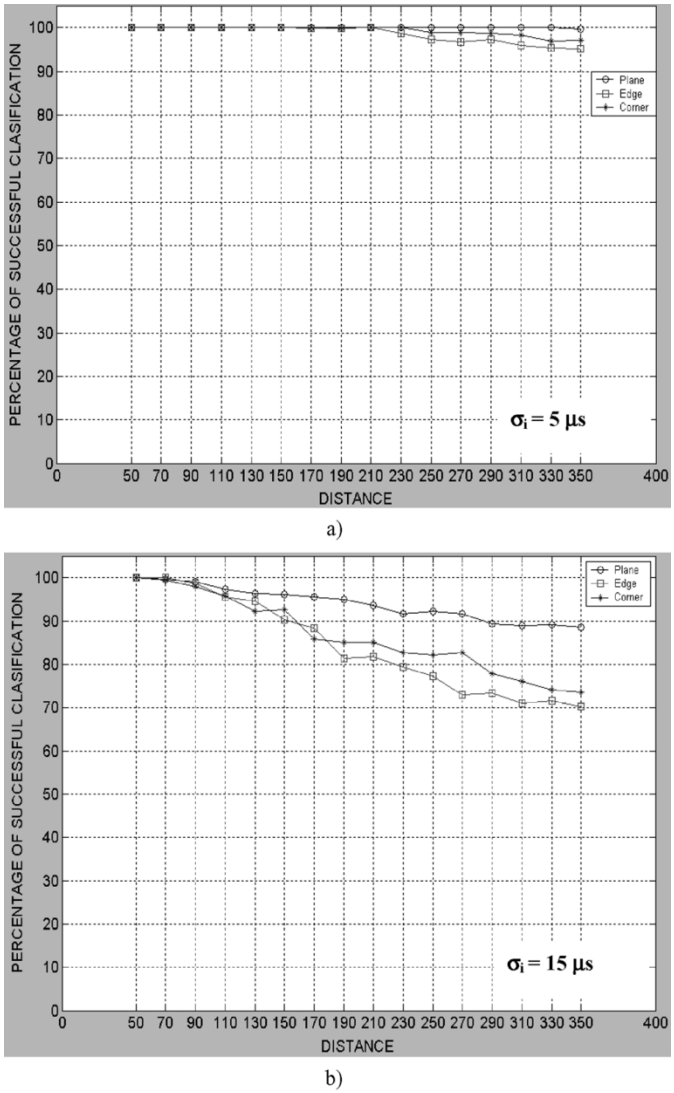

Fig. 9. Success percentage in the classification depending on the distance for plane, edge, and corner-type reflectors placed at distances from 50 to 350 cm, with intervals of 20 cm, an azimuth angle of 7.5°, and TOF measurements with typical noise deviations of (a) 5 μs and (b) 15 μs.

and for every azimuth angle, elevation angles have been evaluated in the same range and with the same interval. Under these conditions, a total of 169 directions for every reflector type have been evaluated. In Table II, the considered directions are shown, depending on the azimuth and elevation angles.

Once obtained, the transformation matrices $\mathbf{U}_i^P$, $\mathbf{U}_i^E$, and $\mathbf{U}_i^C (0 \leq i \leq 168)$ in the 169 directions for every considered reflector, classification can be carried out. For instance, some results are presented, obtained when classifying a plane-type reflector located at 160 cm away from the sensorial structure, with azimuth and elevation angles of $+2^o$ and -4^o, respectively. TOF measurements have been considered with typical noise deviations of 5 μs.

In Tables III, IV, and V, the reconstruction errors ε_i^P, ε_i^E, and ε_i^C are shown (with $i = 0, 1, \ldots, 168$), obtained after projecting in all the spaces corresponding to the three considered reflector types: planes, edges, and corners, respectively.

As derived from Tables III, IV, and V, the smallest reconstruction error is obtained for the case of plane-type reflectors for azimuth and elevation angles of $+2^o$ and -4^o, respectively. Therefore, according to the ILPCA algorithm, the reflector belongs to the plane class with azimuth of $+2^o$ and elevation of -4^o, which is exactly the case of the analyzed reflector.

A similar reasoning can be made for the cases where the reflector to be classified is an edge or a corner.

Once classified, the distance between the reflector and the sensor is estimated. The Euclidean distances $d_{i_a j}$ are calculated in the transformed space, among the feature vectors $\mathbf{\Omega}_{i_a j}$ for the pattern reflectors from the class to which the classified reflector belongs; in this case, plane class with $+2^o$ azimuth and -4^o elevation, and the feature vector $\mathbf{\Omega}_{\boldsymbol{\tau} i_a}$ of the reflector that is being classified. This distance first allows knowing the nearest pattern reflector which is being classified. As 11 patterns have been used per class, 11 Euclidean distances are obtained, as is presented in Table VI.

In order to obtain the distance ρ at which the reflector is, the interval of distances where the reflector is placed is obtained. From Table VI, it is deduced that the reflector is in the interval

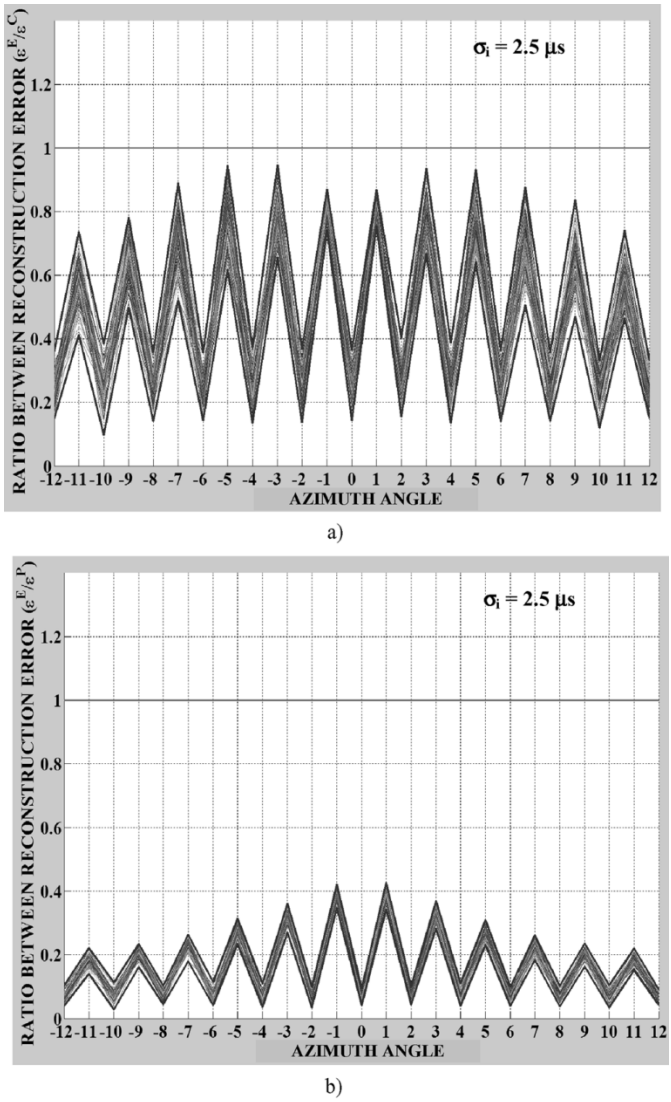

Fig. 10. Ratios between reconstruction errors (a) $\varepsilon^E_{i_{\min}}/\varepsilon^C_{i_{\min}}$ and (b) $\varepsilon^E_{i_{\min}}/\varepsilon^P_{i_{\min}}$, considering measurements with standard noise deviations of 2.5 μs, reflectors placed at 150 cm, and azimuth angles from -12 to $+12$ degrees (elevation angle is zero here).

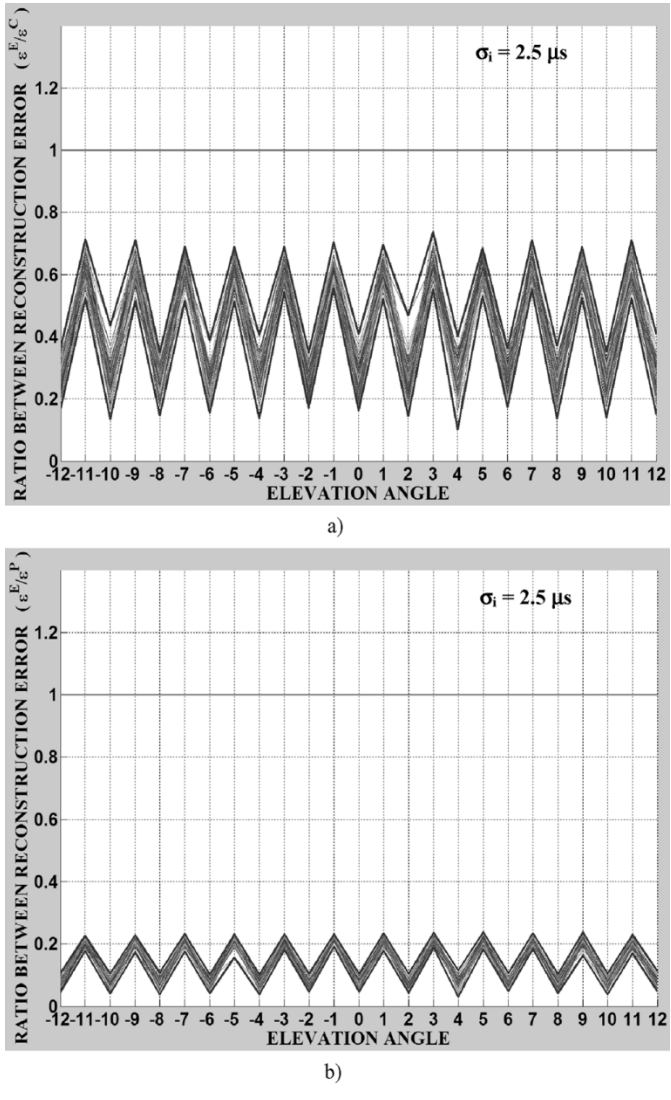

Fig. 11. Ratios between reconstruction errors (a) $\varepsilon^E_{i_{\min}}/\varepsilon^C_{i_{\min}}$ and (b) $\varepsilon^E_{i_{\min}}/\varepsilon^P_{i_{\min}}$, considering measurements with standard noise deviations of 2.5 μs, reflectors placed at 150 cm, and elevation angles from -12 to $+12$ degrees (azimuth angle is zero here).

from 140 to 170 cm, since the smaller Euclidean distances have been obtained in this interval. Finally, the most accurate approach to the distance is obtained by carrying out the linear interpolation according to (27). In this case, keeping in mind the obtained interval, the value ρ can be determined by means of the following expression:

$$\rho = 170 + \frac{140-170}{||\mathbf{\Omega}_{140} - \mathbf{\Omega}_{170}||}||\mathbf{\Omega}_{\boldsymbol{\tau}} - \mathbf{\Omega}_{170}|| = 159.99\,\text{cm}. \quad (28)$$

With the result obtained in (28), it is shown how the relationship among Euclidean distances in the transformed space, and the distances at which the reflectors are with regard to the sensorial structure, follows an approximately linear variation, since the obtained distance $\mathrm{r} = 159.99$ cm coincides with the distance at which the classified reflector is (160 cm).

When repeated, this analysis for different types of reflectors and in different distance locations, azimuth, and elevation, gives successful results, as well.

During the experimental tests, due to problems in practical implementation, all the measurements have been carried out on reflectors with null elevation, only keeping in mind their distance and azimuth with regard to the sensorial structure. Several simulations have been carried out to check the behavior of the ILPCA algorithm, depending on variations in distance and azimuth. In order to verify their behavior at a distance, reflectors located at intervals of 20 cm have been considered, in the range from 50 to 350 cm, with a fixed azimuth angle of 7.5°. The reflectors have been located at 20-cm intervals with the purpose of not being exactly the same as the pattern reflectors located in the same range, but at 30-cm intervals. In this way, more critical classification situations can be proposed, which allows the robustness of the algorithm to be checked in a more intensive way. In order to check their sensitivity with regard to the azimuth angle variations, reflectors have been located at a fixed distance of 150 cm, whereas this angle has been varied from $+12°$ to $-12°$, with intervals of $1°$. The classification errors have been calculated in every position. All the simulations have

been carried out for TOF measurements with Gaussian noise of null mean and typical deviations of 2.5 μs, 5 μs, and 15 μs.

When considering null elevation, the number of directions to be considered in order to obtain the transformation matrices $\mathbf{U}_i^P$, $\mathbf{U}_i^E$, and $\mathbf{U}_i^C$ is reduced to 13 ($i = 0, 1, \ldots, 12$), keeping in mind that angles are evaluated from -12 to $+12$ degrees, at intervals of 2°.

After computing the corresponding reconstruction errors, the ratios $\varepsilon_{i_{\min}}^P/\varepsilon_{i_{\min}}^E$, $\varepsilon_{i_{\min}}^P/\varepsilon_{i_{\min}}^C$, $\varepsilon_{i_{\min}}^E/\varepsilon_{i_{\min}}^P$, $\varepsilon_{i_{\min}}^E/\varepsilon_{i_{\min}}^C$, and $\varepsilon_{i_{\min}}^C/\varepsilon_{i_{\min}}^P$, $\varepsilon_{i_{\min}}^C/\varepsilon_{i_{\min}}^E$ are obtained for every distance, and represented in Figs. 6, 7, and 8, respectively. These results have been obtained after carrying out 500 measurements considering variations in reflector distance, and measurements with typical noise deviations of 2.5 μs. The zig-zag shape of the curves in these figures is because the further the reflectors to be classified (online process) are situated from the pattern reflector positions used during the training process (offline computing of principal components), the more affected by noise the reconstruction errors are.

As can be observed in Figs. 6–8, in any case, the limit value of the unit is overcome, so the success percentage is 100% for any reflector type and for any distance inside the considered range. In the same figures, it is shown that as the the distance increases, the ratios approach the decision threshold, so the classification becomes more critical. This occurs because increasing the distance results in more similar measurements obtained for any reflector type, and they are determined with smaller precision, making the classification difficult.

On the other hand, the worst behavior takes place for the ratios $\varepsilon_{i_{\min}}^P/\varepsilon_{i_{\min}}^E$, $\varepsilon_{i_{\min}}^P/\varepsilon_{i_{\min}}^C$, $\varepsilon_{i_{\min}}^E/\varepsilon_{i_{\min}}^P$, $\varepsilon_{i_{\min}}^E/\varepsilon_{i_{\min}}^C$, and $\varepsilon_{i_{\min}}^C/\varepsilon_{i_{\min}}^P$, $\varepsilon_{i_{\min}}^C/\varepsilon_{i_{\min}}^E$. In these cases, values taken by the ratios are nearer than in others, mainly in the last two cases. Therefore, as the noise level increases in the measurements, a larger classification error appears in these cases.

In Fig. 9(a) and (b), the success percentages are shown for edge, corner, and plane-type reflectors, located at different distances, and with an azimuth angle of 7.5°, considering typical noise deviations of 5 μs and 15 μs, respectively.

As is derived from Fig. 9(a), when the noise in a typical deviation in the measurements is 5 μs, the success percentage for plane-type reflectors is 100%, causing errors to appear in the classification for edge and corner-type reflectors. Whenever the noise has a typical deviation of 15 μs [Fig. 9(b)], the likelihood of success drops significantly. It should be remarked that these so-high typical deviations seldom appear in practice. The purpose of obtaining results with such high levels of noise is to check the behavior of the algorithms in extreme situations.

In order to test the ILPCA algorithm sensitivity to variations in the azimuth and elevation angles, reflectors were placed at a fixed distance, whereas the azimuth or elevation angles were varied. These variations were taken in the range from -12 to $+12$ degrees, with a step of one degree. This test shows that the percentage of successful classifications, for every tested distance, is similar in the whole range of azimuth or elevation angles. Therefore, it can be concluded that the azimuth or elevation angle of the reflector does not have a significant influence on the classification process. Thus, the percentage of successful classifications depends mainly on the distance.

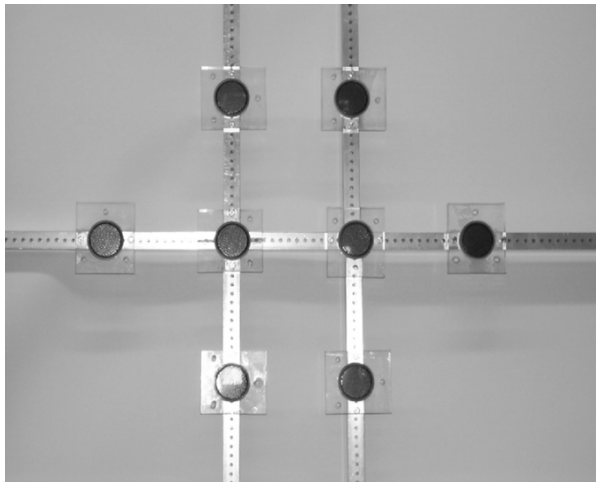

Fig. 12. Sensorial structure used for the experimental tests.

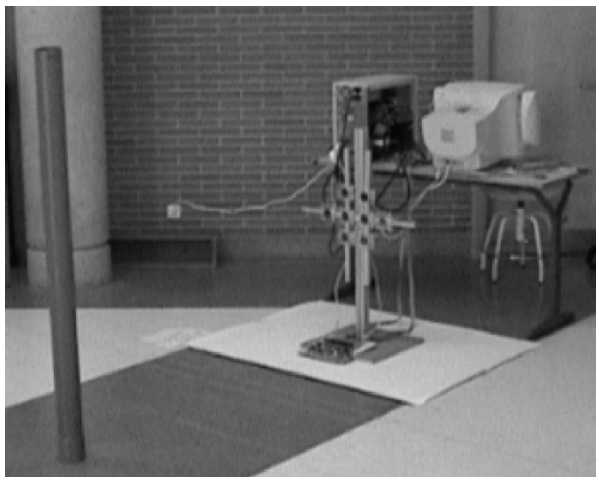

Fig. 13. Test scenario for an edge-type reflector.

As an example, Figs. 10 (variations in azimuth) and 11 (variations in elevation) show values obtained for the following relations: $\varepsilon_{i_{\min}}^E/\varepsilon_{i_{\min}}^C$ and $\varepsilon_{i_{\min}}^E/\varepsilon_{i_{\min}}^P$, after carrying out 500 measurements with standard noise deviations of 2.5 μs, reflectors placed at 150 cm, and angles from -12 to $+12$ degrees with a step of one degree. As can be observed in the figures, there is no case in which the decision threshold (the ratio between reconstruction errors equals one) is overcome. The reason for the maximum peaks shown in the graphics of Figs. 10 and 11 for odd angles, is that in those positions, there were no reflectors placed during the offline process to obtain the transformation matrices (during the offline process, the training reflectors were placed in the range $+12$ to -12° with a two-degree step).

The same conclusions are obtained for all the other relations, $\varepsilon_{i_{\min}}^P/\varepsilon_{i_{\min}}^E$, $\varepsilon_{i_{\min}}^P/\varepsilon_{i_{\min}}^C$ and $\varepsilon_{i_{\min}}^C/\varepsilon_{i_{\min}}^P$, $\varepsilon_{i_{\min}}^C/\varepsilon_{i_{\min}}^E$.

Regarding the separation of the transducers, it is important to remark that the distance reduction, which provides a better behavior of the echo correspondence, also reduces the maximum classification distance. For instance, with a transducer separation of 10 cm, the classification success percentages start to degrade considerably for reflectors located at distances further away than 110 cm.

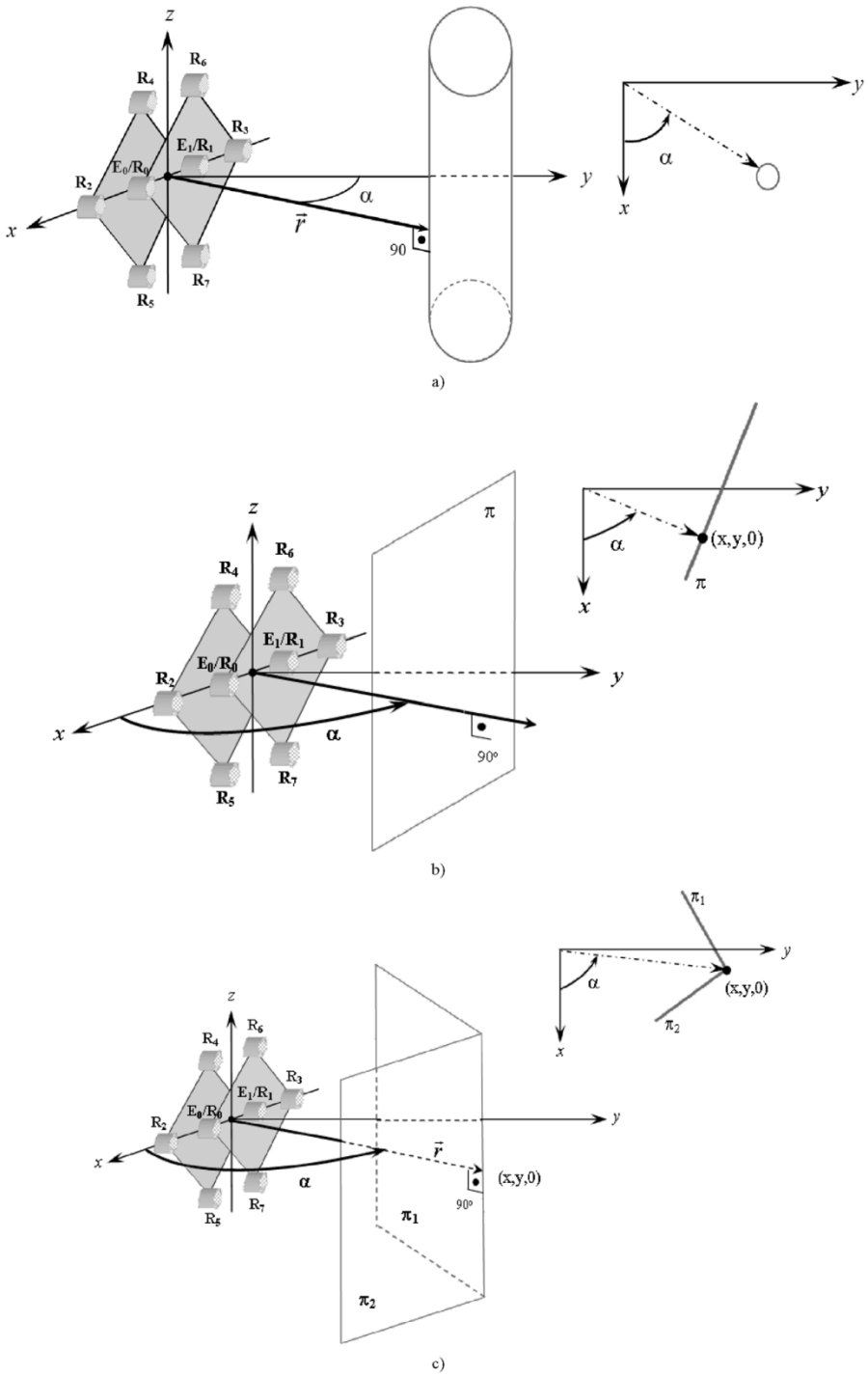

Fig. 14. Position of the three reflector types, (a) edges, (b) planes, and (c) corners, for the experimental tests.

Although all the results presented come from simulations done with noncorrelated noise, tests with correlated noise have been carried out. It has been verified that the proposed algorithm is very robust against that kind of noise. In these tests, the classification is successful, even when the correlated noise has higher standard deviations than the noncorrelated noise.

B. Experimental Results

In order to obtain experimental results, the following resources have been used: a sensor formed by eight transducers (see Fig. 12), where only the two central transducers work as emitters/receivers, whereas the others work as receivers; an edge-type reflector (PVC cylindrical tube of 9-cm diameter); one plane-type (244×122 cm wooden board); and another corner-type (two 244×122 cm wooden boards forming an angle of 90°). Fig. 13 shows the test scenario for an edge-type reflector. The transducers used to build up the sensor system are by Polaroid. This choice is justified by the low cost, high distance range, and bandwidth capabilities (allowing the signal codification). Concerning the measurement system, the

TABLE VII
SUCCESS PERCENTAGE FOR THE ILPCA CLASSIFIER, OBTAINED FOR AN EDGE-TYPE REFLECTOR (CYLINDER WITH A DIAMETER OF 9 cm)

LOCATION	EDGE	CORNER	PLANE	INDETERMINATE
x=70 cm α=0°	100%	0%	0%	0%
x=70 cm α=+4°	99%	1%	0%	0%
x=150 cm α=0°	94%	6%	0%	0%
x=150 cm α=+4°	92%	8%	0%	0%
x=300 cm α=0°	85%	14%	1%	0%
x=300 cm α=-4°	84%	15%	1%	0%

TABLE VIII
SUCCESS PERCENTAGE FOR THE ILPCA CLASSIFIER, OBTAINED FOR A PLANE-TYPE REFLECTOR (244×122-cm WOODEN BOARD)

LOCATION	EDGE	PLANE	CORNER	INDETERMINATE
x=70 cm α=0°	0%	100%	0%	0%
x=70 cm α= +7°	0%	100%	0%	0%
x=150 cm α=0°	1%	99%	0%	0%
x=150 cm α= +7°	2%	98%	0%	0%
x=300 cm α=0°	3%	96%	1%	0%
x=300 cm α= +7°	5%	94%	1%	0%

TABLE IX
SUCCESS PERCENTAGE FOR THE ILPCA CLASSIFIER, OBTAINED FOR A CORNER-TYPE REFLECTOR (TWO 244×122-cm WOODEN BOARDS FORMING 90°)

LOCATION	EDGE	PLANE	CORNER	INDETERMINATE
x=70 cm α=0°	1%	0%	99%	0%
x=150 cm α=0°	7%	1%	92%	0%
x=300 cm α=0°	14%	3%	83%	0%

standard deviation of the TOF measurements is approximately 3 μs for 300-cm distances. More detailed characteristics of the measurement system can be found in [30].

The fact of using a sensor formed by eight transducers for the experimental tests, instead of the 14 transducers originally proposed, is due to the constraint imposed by the number of channels in the acquisition system used. This fact influences the quality of the results, since the effectiveness of the PCA techniques increases as the amount of available data does.

For the experimental tests, the three reflector types have been located at different distances and with different orientations in azimuth, with regard to the sensor. The position of every reflector is determined by two variables, as can be observed in Fig. 14: the distance (module of the vector $\vec{r}$) and angle in azimuth α. In these tests, the elevation of the reflectors has not been taken into account, due to the problems in physical location for the used reflectors.

The measurements considered correspond always to the first echo received. A correspondence analysis (taking the readings two by two) [4], [20] is carried out previous to the application of the ILPCA algorithm. The measurements not passing the correspondence condition are updated to the averaged value from the ones meeting this condition. Only isolated reflectors have been considered, although in future work, more realistic scenarios will be studied. The field of view for the whole sensorial system depends on the view angle from a transducer (20° for the Polaroid transducer), but there is a dead zone of 75 cm approximately just in front of the sensor.

In Tables VII–IX, the success percentages are shown, obtained for every reflector type after carrying out 200 measurements from every location.

From the obtained results, it can be concluded that the classification is degraded as the distance between the reflector and the sensor increases, as happens in simulations. This is due to the greater similarities among the measurements for the three types of reflectors, and to the greater margin of error that appears in the TOF determination. On the other hand, it can be demonstrated that the best results are obtained for the plane-type reflectors. This feature is due to the larger amount of energy that this reflector bounces back, which allows a more accurate TOF to be determined.

It has also been verified that the results obtained in simulations and in practical tests with the eight-transducer sensor have a high degree of similarity when typical noise deviations of 5 μs are considered in simulations (the practical system presents deviations next to 3 μs). Therefore, the practical results obtained using a sensor with 14 transducers should be similar to those obtained in simulations, shown in Section IV-A.

V. CONCLUSIONS AND FUTURE WORK

In this paper, a sensorial structure and a classification algorithm based on the PCA techniques have been proposed, with which three types of basic 3-D reflectors can be classified: planes, corners, and edges.

Regarding the sensorial structure, it is necessary to remark the features different from other proposals carried out by other authors in previous work in the same line: their capacity to obtain 3-D information from the environment, the high redundancy provided, and their capacity for simultaneous emission/reception. These characteristics make it suitable for use as a sensorial system in mobile robot applications.

When considering the classification algorithm, it should be noted that the classification is carried out using only TOFs measured by the different transducers in the sensorial structure. The excellent behavior of the proposed classification algorithm (ILPCA) for a wide range of distances has been demonstrated by means of simulations and experimental tests, even under extreme noise conditions in measurements.

In this system, even with a success rate in reflector classification similar to other algorithms proposed in the literature, the robustness against false readings is improved. Furthermore, the

ILPCA algorithm is a compact process of information integration for all the readings determined in only one measurement cycle. Also, it can be easily adapted to any number of transducers in the sensorial system. In this case, the redundancy is considered at the level of measurements (simultaneously obtained), and not in high-level algorithms which integrate the information from successive readings.

As future work, the sensorial system will be adapted and tested on a mobile robot in real scenarios. Obviously, in these complex scenarios, it is necessary to implement high-level tasks: correspondence analysis of echoes, reflector segmentation, SLAM algorithms, etc.

REFERENCES

[1] R. Kuc and Y. Di, "Intelligent sensor approach to differentiating sonar reflections from corners and planes," in *Proc. Int. Congr. Intell. Auton. Syst.*, Amsterdam, The Netherlands, 1986, pp. 329–333.

[2] B. Barshan and R. Kuc, "Differentiating sonar reflections from corners and planes by employing an intelligent sensor," *IEEE Trans. Pattern Anal. Machine Intell.*, vol. 12, no. 6, pp. 560–569, Jun. 1990.

[3] J. J. Leonard and H. F. Durrant-Whyte, "Mobile robot localization by tracking geometric beacons," *IEEE Trans. Robot. Autom.*, vol. 7, no. 3, pp. 376–382, Jun. 1991.

[4] L. Kleeman and R. Kuc, "Mobile robot sonar for target localization and classification," *Int. J. Robot. Res.*, vol. 14, no. 4, pp. 295–318, Aug. 1995.

[5] P. J. McKerrow and J. C. T. Hallam, "An introduction to the physics of echolocation," in *Proc. 3rd Nat. Conf. Robot.*, Melbourne, Australia, 1990, pp. 198–209.

[6] A. M. Sabatini, "Active hearing for external imaging based on an ultrasonic transducer array," in *Proc. IEEE/RSJ Int. Conf. Intell. Robots Syst.*, Raleigh, NC, 1992, pp. 829–836.

[7] H. Peremans, K. Audenaert, and J. M. Van Campenhout, "A high-resolution sensor based on tri-aural perception," *IEEE Trans. Robot. Autom.*, vol. 9, no. 1, pp. 36–48, Feb. 1993.

[8] E. G. Araujo and R. A. Grupen, "Feature extraction for autonomous navigation using an active sonar head," in *Proc. IEEE Int. Conf. Robot. Autom.*, San Francisco, CA, Apr. 2000, pp. 3823–3828.

[9] A. Heale and L. Kleeman, "Fast target classification using sonar," in *Proc. IEEE/RSJ Int. Conf. Intell. Robots Syst.*, Maui, HI, Oct. 2001, pp. 1446–1451.

[10] Y. Han and H. Hahn, "Localization and classification of target surfaces using two pairs of ultrasonic sensors," in *Proc. IEEE Int. Conf. Robot. Autom.*, Detroit, MI, May 1999, pp. 637–643.

[11] S. W. Utete, B. Barshan, and B. Ayrulu, "Voting as validation in robot programming," *Int. J. Robot. Res.*, vol. 18, no. 4, pp. 401–413, 1999.

[12] H. J. Jeon and B. K. Kim, "A study on world map building for mobile robots with tri-aural ultrasonic sensor system," in *Proc. IEEE Int. Conf. Robot. Autom.*, 1995, pp. 2907–2912.

[13] N. A. Oufroukh, C. Barat, and E. Colle, "Distinction between objects with ultrasonic biaural system and only amplitude," in *Proc. IEEE Int. Conf. Emerging Technol. Factory Autom.*, 2001, pp. 757–760.

[14] B. Ayrulu, B. Barshan, and S. W. Utete, "Target identification with multiple logical sonars using evidential reasoning and simple majority voting," in *Proc. IEEE Int. Conf. Robot. Autom.*, 1997, pp. 2063–2068.

[15] B. Ayrulu and B. Barshan, "Neural network for improved target differentiation and localization with sonar," *Neural Netw.*, vol. 14, no. 3, pp. 355–373, 2001.

[16] ——, "Reliability measure assignment to sonar for robust target differentiation," *Pattern Recog.*, vol. 35, no. 6, pp. 1403–1419, 2002.

[17] D. Diep, A. Johannet, P. Bonnefoy, F. Harroy, and P. Loiseau, "Classification of sonar data for a mobile robot using neural networks," in *Proc. IEEE Int. Joint Symp. Intell. Syst.*, 1998, pp. 257–260.

[18] C. Barat and N. A. Oufroukh, "Classification of indoor environment using only one ultrasonic sensor," in *Proc. IEEE Instrum. Meas. Technol. Conf.*, Budapest, Hungary, May 2001, pp. 1750–1755.

[19] H. Peremans and J. M. Van Campenhout, "Tri-aural perception on a mobile robot," in *Proc. IEEE Int. Conf. Robot. Autom.*, Atlanta, GA, 1993, pp. 265–270.

[20] J. Ureña, "Contribución al diseño e implementación de un sistema sonar para la automatización de un vehículo industrial," Ph.D. dissertation (in Spanish), University of Alcala, Madrid, Spain, Feb. 1998.

[21] H. Akbarally and L. Kleeman, "A sonar sensor for accurate 3-D target localization and classification," in *Proc. IEEE lnt. Conf. Robot. Autom.*, Nagoya, Japan, 1995, pp. 3003–3008.

[22] M. L. Hong, "Three-dimensional ultrasonic sensing for autonomous vehicles," Ph.D. dissertation, Nat. Univ. Singapore, Singapore, Feb. 1995.

[23] V. Díaz, J. Ureña, M. Mazo, J. J. García, E. Bueno, and A. Hernández, "Using complementary sequences for multi-mode ultrasonic operation," in *Proc. 7th IEEE Int. Conf. Emerging Technol. Factory Applicat.*, Barcelona, Spain, 1999, pp. 599–604.

[24] A. Hernández, J. Ureña, J. J. García, M. Mazo, J. P. Dérutin, and J. Serot, "Ultrasonic sensor performance improvement using DSP-FPGA based architectures," in *Proc. 28th IEEE Annu. Int. Conf. Ind. Electron., Control, Instrum.*, Seville, Spain, 2002, pp. 2694–2699.

[25] M. Turk and A. Pentland, "Eigenfaces for recognition," *J. Cognit. Neurosci.*, vol. 3, pp. 72–85, 1991.

[26] D. L. Swets and J. J. Weng, "Using discriminant eigenfeatures for image retrieval," *IEEE Trans. Pattern Anal. Machine Intell.*, vol. 18, no. 8, pp. 831–836, Aug. 1996.

[27] M. Kirby and L. Sirovich, "Application of the Karhunen–Loeve procedure for the characterization of human faces," *IEEE Trans. Pattern Anal. Machine Intell.*, vol. 12, no. 1, pp. 103–108, Jan. 1990.

[28] A. Howard, C. Padgett, and C. C. Liebe, "A multi-stage network for automatic target detection," in *Proc. IEEE Int. Joint Conf. Neural Netw., IEEE World Congr. Computat. Intell.*, vol. 1, May 1998, pp. 231–236.

[29] W. Soares-Filho, J. M. Seixas, and L. Caloba, "Principal component analysis for classifying passive sonar signals," in *Proc. IEEE Int. Symp. Circuits Syst.*, Sydney, Australia, 2001, pp. 1–4.

[30] A. Hernández, J. Ureña, J. J. García, M. Mazo, D. Hernanz, J. P. Dérutin, and J. Sérot, "Ultrasonic ranging sensor using simultaneous emissions from different transducers," *IEEE Trans. Ultrason., Ferroelectr., Freq. Control*, vol. 51, no. 12, pp. 1660–1670, Dec. 2004.

[31] L. Kleeman, "Advanced sonar with velocity compensation," *Int. J. Robot. Res.*, vol. 23, no. 2, pp. 111–126, Feb. 2004.

[32] ——, "Advanced sonar and odometry error modeling for simultaneous localization and map building," in *Proc. IEEE/RSJ Int. Conf. Intell. Robots Syst.*, Las Vegas, NV, 2003, pp. 699–704.

[33] H. Peremans, A. Walker, and J. C. T. Hallam, "3-D object localization with a binaural sonarhead, inspirations from biology," in *Proc. IEEE Int. Conf. Robot. Autom.*, Leuven, Belgium, 1998, pp. 2795–2800.

[34] D. L. Swets and J. J. Weng, "Using discriminant eigenfeatures for image retrieval," *IEEE Trans. Pattern Anal. Machine Intell.*, vol. 18, no. 8, pp. 831–836, Aug. 1996.

[35] Y. Mami and D. Charlet, "Speaker identification by anchor models with PCA/LDA post-processing," in *Proc. IEEE Int. Conf. Acoust., Speech, Signal Process.*, vol. 1, Lannion, France, 2003, pp. 180–183.

[36] H. Murase, F. Kimura, M. Yoshimura, and Y. Miyake, "An improvement of the autocorrelation matrix, pattern matching method and its application to handprinted "HIRAGANA"," *Trans. IECE Jpn.*, vol. 64D, no. 3, pp. 276–283, 1981.

[37] W. Soares-Filho, J. M. Seixas, and L. Caloba, "Principal component analysis for classifying passive sonar signals," in *Proc. IEEE Int. Symp. Circuits Syst.*, Sydney, Australia, 2001, pp. 1–4.

José A. Jiménez obtained the electronic telecommunication engineering degree in 1996 from the University of Valencia, Valencia, Spain, and the Ph.D. degree from the University of Alcalá, Madrid, Spain, in 2004.

He is currently an Associate Professor of Instrumentation Electronics with the Electronics Department, University of Alcalá. His research areas are multisensor integration, and sensorial systems applied to robotic, instrumentation, and electronic systems for mobile robots.

Manuel Mazo (M'90) received the Ph.D. degree in telecommunications in 1988, and the M.Sc. engineering degree in telecommunications in 1982, both from the Polytechnic University of Madrid, Madrid, Spain.

Currently, he is a Professor with the Electronics Department, University of Alcalá, Madrid, Spain. His research areas are multisensor (ultrasonic, infrared, and artificial vision) integration and electronic control systems applied to railway safety, mobile robots, and wheelchairs for physically disabled people.

Jesús Ureña received the MS degree in telecommunications engineering from the Polytechnical University of Madrid, Madrid, Spain, in 1992, and the Ph.D. degree in telecommunications from the University of Alcalá, Madrid, Spain, in 1998.

Since 1986, he has been a Lecturer with the Electronics Department, University of Alcalá. He has collaborated in several educational and research projects in the area of electronic control and sensorial systems for mobile robots and wheelchairs, and in the area of electronic systems for railways. His current research areas are low-level ultrasonic signal processing, local positioning systems (LPS), and sensory systems for railway safety.

Álvaro Hernández obtained the electronic engineering degree from the University of Alcalá, Madrid, Spain, in 1998, and the Ph.D. degree from the University of Alcalá, Madrid, Spain, and Blaise Pascal University, Clermont-Ferrand, France, in 2003.

He is currently an Associate Professor of Digital Systems with the Electronics Department, University of Alcalá. His research areas are multisensor integration, electronic systems for mobile robots, digital systems, and computing architectures.

Fernando Álvarez obtained the physics degree from the University of Sevilla, Sevilla, Spain, in 1998.

He is currently an Assistant Professor of Control Engineering with the Electronics Department, University of Extremadura, Badajoz, Spain. His research areas are low-level ultrasonic signal processing and sensory systems for railway safety.

Juan Jesüs García obtained the telecommunication engineering degree in 1998 from the University of Valencia, Valencia, Spain.

He has been an Associate Professor of Analog and Digital Electronics with the Electronics Department, University of Alcalá, Madrid, Spain, since 1994. He has worked on several public and private projects related to digital control and sensors systems, and his current areas of interest are mobile robots and multisensor integration.

Enrique Santiso was born in 1966. He received the M.Sc. degree in electrical engineering from the University of Valencia, Valencia, Spain, and the Ph.D. degree in telecommunications from the University of Alcalá, Madrid, Spain.

He joined the Department of Electronics, University of Alcalá, Madrid, Spain, in 1990 as an Associate Professor and Researcher. His interests are in the fields of mobile robots and computer vision.